Equilibrium and out-of-equilibrium realistic phonon self-energy free from overscreening

Andrea Marini ⬤

Istituto di Struttura della Materia and Division of Ultrafast Processes in Materials (FLASHit) of the National Research Council and European Theoretical Spectroscopy Facilities (ETSF), Via Salaria Km 29.3, I-00016 Monterotondo Stazione, Italy

In model Hamiltonians, like Fröhlich's, the electron-phonon interaction is assumed to be screened from the beginning. The same occurs when this interaction is obtained by using the state-of-the-art density functional perturbation theory as starting point. In this work I formally demonstrate that these approaches are affected by a severe overscreening error. By using an out-of-equilibrium many-body technique I discuss how to merge the many-body approach with density functional perturbation theory in order to correct the overscreening error. A symmetric statically screened phonon self-energy is obtained by downfolding the exact Baym-Kadanoff equations. The statically screened approximation proposed here is shown to have the same long-range spatial limit of the exact self-energy and to respect the fluctuation-dissipation theorem. The doubly screened approximation, commonly used in the literature, is shown, instead, to be overscreened, to violate several many-body properties and to have a wrong spatial long-range decay. The accuracy of the proposed approximation is tested against the exact solution of an extended model Fröhlich Hamiltonian and it is applied to a paradigmatic material: MgB_2. I find that the present treatment enhances the linewidths by 57% with respect to what has been previously reported for the anomalous E_{2g} mode. I further discover that the A_{2u} mode is also anomalous (its strong coupling being completely quenched by the overscreened expression). The present results deeply question methods based on state-of-the-art approaches and impact a wide range of fields such as thermal conductivity, phononic instabilities, and nonequilibrium lattice dynamics.

I. INTRODUCTION

The research on the physics induced by electron–phonon (*e-p*) interaction is one of the most prolific topics in materials science and solid state physics. A recent review by Giustino [1] witnesses the countless implications of this interaction on the physics of electrons and phonons, at and out of equilibrium.

The research connected to the *e-p* interaction that is relevant to this work can be roughly divided in two main areas: the *e-p* effect on the electronic and phononic dynamics. In the first family of applications we find the case of the *e-p* induced renormalization of the electronic gap that has been extensively studied from the theoretical [2,3] and numerical [4] sides. We can conclude that most of the fundamental aspects are now clear, even if there is still an active research activity about on how to go beyond the state-of-the-art approximations and describe more advanced effects, like self-trapping [5].

The case of the *e-p* effects on the phonon states is very different. The main reason is that, as it will be clear in the following, while the electrons are natural quantum objects, phonons do not appear in the full many-body (MB) Hamiltonian written in terms of quantized electrons and nuclei. This, indeed, has to be expanded in powers of the atomic displacements that, in turn, define the elemental phonon states. If, however, we look at this procedure from a MB point of view we see that the electrons will react to the atomic displacement and the phonon definition will depend on the electronic response. However, the electronic response emerges dynamically from the solution of the MB problem, while phonons appear directly in the initial Hamiltonian.

This intrinsic difficulty of defining a coherent approach to the phonon physics is reflected in the different theoretical and methodological approaches that have been proposed in the literature. We have model Hamiltonians where phonons are introduced as exact bosons from the beginning and the *e-p* interaction is defined externally on the basis of physical arguments. A well-known example is the Fröhlich Hamiltonian [6–8]. In the case of model Hamiltonians the problem of describing the electronic response to the atomic displacement is ignored by definition.

Another approach is based on density functional theory (DFT) and density functional perturbation theory (DFPT) [9–11]. DFT and DFPT are two electronic density based theories where the description of the electronic screening, connected to the electronic charge oscillation, naturally appears. Indeed, DFPT represents the state-of-the art approach to describe phonon frequencies with results in excellent agreement with the experiments [12]. DFPT is based on the Born-Oppenheimer (BO) and adiabatic approximations and, more importantly, within DFT and DFPT the atoms are treated classically and the Hamiltonian depends parametrically from their positions. The BO approximation allows to decouple the electronic and nuclear dynamics and define the phonons as oscillations of the atoms around the minimum of the BO energy surface. The adiabatic approximation, instead, assumes that the electrons follow adiabatically the nuclear oscillations. An extension of DFPT to include nonadiabatic effects has been proposed in [13].

The last approach is based on many-body perturbation theory (MBPT) [14] where the *e-p* problem can be formally solved exactly by means of diagrammatic methods [3]. MBPT, however, requires the definition of an initial, reference Hamiltonian and, as I will discuss shortly, this step can potentially lead to overscreening effects if not properly done, especially if DFPT is used as starting point.

In this work I present a detailed and complete MB theory of the phonon self-energy starting from the fully quantistic and bare electron-nuclei Hamiltonian. By working on the Keldysh contour I propose a derivation that is valid at the equilibrium and out of the equilibrium. I derive a full set of equation of motions for the 2×2 phonon displacement and momentum propagators and I show how to derive a symmetric equilibrium form. By using this I introduce a static-screening approximation and show that it correctly respects the diagrammatic structure. The doubly screened approximation for the phonon self-energy, commonly used in the literature, is discussed and compared with the present static-screening approximation. The diagrammatic analysis reveals an exploding number of double-counted diagrams and, more importantly, the exact solution of a generalized model Frhölich Hamiltonian clearly show that the doubly screened phonon self-energy has a wrong vanishing momentum limit that leads to a large underestimation of the long-wavelength phonon widths. I conclude this work by applying the static-screening approximation to a paradigmatic material: MgB_2.

The paper is organized as follows: In the following two sections I introduce a heuristic explanation of the physical origin of the overscreening error (Sec. I A) and a review of the existing literature (Sec. I B). The main body of the work starts in Sec. II with a careful derivation of the electron-nuclei Hamiltonian by Taylor expanding the fully quantized *ab initio* Hamiltonian. In Sec. II A I discuss the reference phonon basis and the corresponding electron-nuclei potentials needed to avoid double-counting terms that appear already in the Hamiltonian. I then move to the MBPT approach that is reviewed in Sec. III. In order to derive the equation of motion for the atomic displacement and momentum operators (Sec. III A) and for the corresponding Green's function (Sec. III B) I introduce several key concepts like the vertex function in Sec. III C and the phonon self-energy in Sec. III D.

In Sec. IV I mathematically introduce the equilibrium regime deriving a symmetric form of the Dyson equation suitable to introduce the static screening approximation. After further simplifications in Sec. V B to obtain a form of the self-energy that will be later implemented, I move to the discussion of the key role played by the electronic screening (Sec. V). The partially screened and doubly screened approximations are discussed from a diagrammatic point of view in Sec. V A. In Sec. V C, instead, they are compared with the self-energy derived analytically in an exactly solvable model.

In Sec. VI I discuss how to merge MBPT with methods based on the Born-Oppenheimer approximation, of which DFPT is an example. By using this scheme, in Sec. VII, I calculate the phonon widths of MgB_2. The paper is concluded in Appendix C by describing the code implementation I developed in this work using the QUANTUM ESPRESSO and YAMBO codes, and providing a scheme of the calculation flow (Appendix D).

A. Overscreening error: A heuristic introduction

The origin of the overscreening effect can be heuristically introduced by starting from a well-known concept: the Hartree potential. Let us start from a purely electronic initial Hamiltonian

$$\hat{H} = \hat{H}_e + \hat{H}_{e\text{-}e}, \qquad (1)$$

with $\hat{H}_{e\text{-}e} = \frac{1}{2} \sum_{ij}' v(\hat{\mathbf{r}}_i - \hat{\mathbf{r}}_j)$ and v the **bare** Coloumb interaction. The *e-e* interaction produces, at the lowest order of perturbation theory, a mean field and classical potential: the Hartree potential

$$V_H(\mathbf{r}) = \int d\mathbf{r}' v(\mathbf{r} - \mathbf{r}')\rho(\mathbf{r}'), \qquad (2)$$

with ρ the electronic density. In Eq. (2) the Coulomb interaction is bare. In 1988, Allen, Cohen, and Penn [15] have demonstrated, by using a variational argument, that two test charges in a solid interact through a screened Coulomb interaction $W = \epsilon^{-1} v$, with ϵ the dielectric function of the material. At the same time it is well known that by replacing v with W in Eq. (1) we would get an overscreened Hartree, classical potential. This would be nonphysical and makes impossible to rewrite $\hat{H}$ in terms of W only. $\hat{H}$ must be written in terms of v with its electronic screening being induced by the dynamical solution of the many-body problem.

In the *e-p* case the situation is the same. Let us add to Eq. (1) the *e-p* interaction

$$\hat{H} = \hat{H}_{ph} + \hat{H}_e + \hat{H}_{e\text{-}p} + \hat{H}_{e\text{-}e}, \qquad (3)$$

where $\hat{H}_{ph}$ is the noninteracting phonon system taken in the harmonic approximation with eigenvalues ω_ν. $\hat{H}_{e\text{-}p} = \sum_{ij\nu} g^\nu_{ij} \hat{\rho}_{ij} \hat{u}_\nu$ is the electron-phonon interaction with g^ν_{ij} the *bare* electron-phonon potential, $\hat{u}$ the phonon displacement, and $\hat{\rho}_{ij}$ the electronic density operator.

As I will demonstrate in this work the *e-p* interaction produces, at the same perturbation order of the Hartree potential, a mean field potential $U^\nu \propto g^\nu$ [Eq. (42b)]. It is also well known [1,2,16] that the variation of the Hartree potential screens g^ν. As in the purely electronic case this means that any observable evaluated on the interacting ground state of $\hat{H}$ will be written in terms of g^ν *and* $g^\nu|_{SCR} \sim \epsilon^{-1} g^\nu$. This applies to the electronic gap, optical absorption, and phonon energies and related properties. In practice this means that, in general, *it is not possible* to write

$$\hat{H}_{e\text{-}p} = g^\nu_{ij}|_{SCR} \hat{\rho}_{ij} \hat{u}_\nu, \qquad (4)$$

when $\hat{H}$ contains the *e-e* interaction, even at a mean field level. In this case Eq. (4) inevitably produces an overscreened error.

B. Literature review

In 1972 Allen published a work about superconductivity [17] where he derived a relation between the Eliashberg function $\alpha^2 F(\omega)$ and the phonon widths [Eq. 9 of [17]]. As the $\alpha^2 F(\omega)$ is known to be proportional to $(g^\nu|_{SCR})^2$ Allen formulation suggested that also the phonon widths have the same proportionality. Allen's expression for the Eliashberg function has been applied to evaluate the superconductive properties of materials in, for example, Refs. [18,19].

I will explain in Sec. VIII 2 that the Allen's expression is affected by a conceptual error, as it is true only if Eq. (4) is used. This limitation was already pointed out by Allen himself in 1983 [20] where he wrote the following: *"The essence of the Fröhlich Hamiltonian is that Coulomb interactions have already renormalized the electronic energies and e-p interaction, and both Coulomb and electron-phonon interactions have renormalized the phonon frequencies. This Hamiltonian is now used to construct the electronic self-energy. It cannot be used to construct the phonon self-energy because the phonon frequency is already the observed renormalized spectrum."*

Nevertheless, the expression of the phonon widths proportional to $(g^\nu|_{\mathrm{SCR}})^2$ has been extensively used in the literature to calculate a wealth of properties. This is especially true in DFT and DFPT based methods where $g^\nu|_{\mathrm{SCR}}$ is a natural by-product of any adiabatic phonon calculations. Nevertheless, within DFT and DFPT the *e-e* interaction is replaced with the Kohn-Sham (KS) Hartree plus exchange-correlation potential. As this potential includes the Hartree terms it follows that the *e-p* interaction is screened. Indeed, within DFPT phonon frequencies are adiabatically renormalized by the electronic response. Despite this many authors have calculated phonon-related properties by using Eq. (4) and, thus, overscreening the *e-p* interaction. Overscreened calculations have been performed of (i) the lattice thermal conductivity and transport [21–24], (ii) nonadiabatic phonon corrections, linewidths and Kohn anomalies [13,25–36], out-of-equilibrium phonon dynamics [37–41].

While MBPT studies [2,16,42] provide a coherent scheme in the DFPT community, there is no unique consensus on the procedure to use to correctly screen the *e-p* interaction. While some authors [43–46] have proposed a partially screened form of the dynamical matrix, in Ref. [13] the authors presented variational arguments in favor of the fully screened formulation.

II. DEFINITION OF THE *AB INITIO* ELECTRON-PHONON HAMILTONIAN

The starting Hamiltonian is a key ingredient of the entire derivation. Indeed, a proper definition of the different potentials that appear once the nuclear and electron-nuclei interaction are Taylor expanded is mandatory to have a well-defined *e-p* Hamiltonian. In this section I review and extend to the phonon case the procedure introduced in Ref. [3].

I start from the generic form of the total Hamiltonian of the system, that I divide in electronic $\hat{H}_e$, nuclear $\hat{H}_n$, and electron-nucleus (*e-n*) $\hat{H}_{e\text{-}n}$ contribution. I keep all components, electrons and nuclei, quantized:

$$\widehat{H} = \hat{H}_e + \hat{H}_n + \hat{H}_{e\text{-}n}. \qquad (5)$$

The electronic and nuclear parts are divided in a kinetic $\widehat{T}$ and interaction part $\widehat{W}$:

$$\hat{H}_e = \hat{T}_e + \hat{H}_{e\text{-}e}, \qquad (6a)$$

$$\hat{H}_n = \hat{T}_n + \hat{H}_{n\text{-}n}. \qquad (6b)$$

Note that the nuclear kinetic energy depends on the nuclear momenta. In the above definitions, the operators are bare (undressed).

The explicit expression for the bare (*e-n*) interaction term is

$$\hat{H}_{e\text{-}n} = -\sum_{I,i} Z_I v(\hat{\mathbf{r}}_i - \hat{\mathbf{R}}_I) = \sum_{I,i} V_{e\text{-}n}(\hat{\mathbf{r}}_i, \hat{\mathbf{R}}_I), \qquad (7)$$

where $\hat{\mathbf{R}}_I$ is the nuclear position operator for the Ith nucleus, Z_I is the corresponding charge, $\hat{\mathbf{r}}_i$ is the electronic position operator of the electron i, and $v(\mathbf{r} - \mathbf{r}') = |\mathbf{r} - \mathbf{r}'|^{-1}$ is the bare Coulomb potential. Similarly,

$$\hat{H}_{n\text{-}n} = \frac{1}{2} {\sum_{I,J}}' Z_I Z_J v(\widehat{\mathbf{R}}_I - \widehat{\mathbf{R}}_J) = \frac{1}{2} {\sum_{I,J}}' V_{n\text{-}n}(\hat{\mathbf{R}}_I, \hat{\mathbf{R}}_J) \qquad (8a)$$

and

$$\hat{H}_{e\text{-}e} = \frac{1}{2} {\sum_{ij}}' v(\widehat{\mathbf{r}}_i - \widehat{\mathbf{r}}_j), \qquad (8b)$$

with $\sum'_{ij} = \sum_{i \neq j}$.

I now split the nuclear position operator $\hat{\mathbf{R}}_I$ in reference and displacement

$$\hat{\mathbf{R}}_I = \overline{\mathbf{R}}_I + \hat{\mathbf{u}}_I, \qquad (9)$$

and now use the notation $\overline{O(\hat{\mathbf{R}})}$ to indicate a quantity or an operator that is evaluated with the nuclei frozen in their reference crystallographic positions ($\overline{\mathbf{R}}$).

Note that the reference atomic positions are not restricted to correspond to the equilibrium lattice geometry. A more formally correct definition of equilibrium condition will be given in Sec. II A when I will define the reference residual atomic force and dynamical matrix.

At this point I can formally introduce the electron-phonon interaction be Taylor expanding Eq. (8) up to second order in the quantized nuclear displacements:

$$\hat{H}_{\mathrm{kind}} = \overline{\hat{H}}_{\mathrm{kind}} + \sum_I \overline{\nabla_I \hat{H}_{\mathrm{kind}}} \cdot \hat{\mathbf{u}}_I + \frac{1}{2} {\sum_{I,J}}' \hat{\mathbf{u}}_I$$
$$\cdot \overline{\nabla_I \nabla_J \hat{H}_{\mathrm{kind}}} \cdot \hat{\mathbf{u}}_J, \qquad (10)$$

where kind = *e-n, n-n*. While in the *e-n* case $\overline{\hat{H}_{\mathrm{kind}}}$ is an operator, in the *n-n* case it is a *C* number.

In order to define a Hamiltonian suitable to apply MBPT we need a reference basis for the phonon modes. The procedure to introduce this reference is explained in Secs. III–IV of Ref. [3]. In the following I review and extend it to the present context.

I start by introducing a reference tensorial dynamical matrix $\overleftrightarrow{C}_{IJ}^{\mathrm{ref}}$ which, in turns, define a reference Hamiltonian

$$\hat{H}_{\mathrm{ref}} = \frac{1}{2} {\sum_{IJ}}' \hat{\mathbf{u}}_I \cdot \overleftrightarrow{C}_{IJ}^{\mathrm{ref}} \cdot \hat{\mathbf{u}}_J. \qquad (11)$$

Equation (11) defines the corresponding phonon basis via standard canonical transformation. Indeed, if $\boldsymbol{\xi}_{I\lambda}$ is the rotation matrix to diagonalize $\overleftrightarrow{C}^{\mathrm{ref}}$ we get

$$\sum_{JL} \boldsymbol{\xi}_{J\lambda}^T \cdot \frac{\overleftrightarrow{C}_{JL}^{\mathrm{ref}}}{\sqrt{M_J M_L}} \cdot \boldsymbol{\xi}_{L\lambda'} = \delta_{\lambda\lambda'} \omega_\lambda^2. \qquad (12)$$

To keep the notation compact in this section I will use λ to indicate a phonon branch and momentum. Thanks to Eq. (12) I can define the reference phonon displacement and momentum

operators as components of a vectorial operator $\hat{\phi}$:

$$\hat{\phi}_{s\lambda} = \begin{cases} \frac{1}{\sqrt{2}}(\hat{b}_\lambda^\dagger + \hat{b}_\lambda), & s = + \\ \frac{i}{\sqrt{2}}(\hat{b}_\lambda^\dagger - \hat{b}_\lambda), & s = - \end{cases} \tag{13}$$

with $\hat{b}_\lambda^\dagger$ the phonon λ creation operator. It follows that

$$\hat{\mathbf{u}}_I = \sum_\lambda \frac{1}{\sqrt{M_I \omega_\lambda}} \boldsymbol{\xi}_{I\lambda} \hat{\phi}_{+\lambda}, \tag{14a}$$

$$\hat{\mathbf{p}}_I = \sum_\lambda \sqrt{\frac{\omega_\lambda}{M_I}} \boldsymbol{\xi}_{I\lambda} \hat{\phi}_{-\lambda}. \tag{14b}$$

Thanks to Eq. (14) it is possible to write that

$$\hat{T}_n + \hat{H}_{\text{ref}} = \sum_{s\lambda} \frac{\omega_\lambda}{2} \hat{\phi}_{s\lambda}^\dagger \hat{\phi}_{s\lambda}. \tag{15}$$

The last step we need to introduce the *e-p* Hamiltonian is to move in second quantization

$$\hat{H}_{e\text{-}p} = \hat{H}_{e\text{-}n} - \overline{\hat{H}_{e\text{-}n}} = \sum_I \int d\mathbf{r}_1 \hat{\rho}(\mathbf{r}_1) \boldsymbol{\nabla}_I V_{e\text{-}n}(\mathbf{r}_1, \overline{\mathbf{R}}_I) \cdot \hat{\mathbf{u}}_I, \tag{16}$$

where $\hat{\rho}(\mathbf{r}) = \hat{\psi}^\dagger(\mathbf{r})\hat{\psi}(\mathbf{r})$ and $\hat{\psi}(\mathbf{r}) = \frac{1}{\sqrt{N}} \sum_i \phi_i(\mathbf{r})\hat{c}_i$, with N the number of points used to sample the Brillouin zone,[1] and $\phi_i(\mathbf{r})$ the reference electronic wave function of the state i.

I now use Eq. (14) to write the *e-p* interaction term in the reference phonon basis

$$\hat{H}_{e\text{-}p} - \overline{\hat{H}_{e\text{-}n}} = \sum_\lambda \int d\mathbf{r}_1 \hat{\rho}(\mathbf{r}_1) g^\lambda(\mathbf{r}_1)\hat{\phi}_{+\lambda}, \tag{17}$$

with

$$g^\lambda(\mathbf{r}_1) = \sum_I \frac{1}{\sqrt{M_I \omega_\lambda}} \boldsymbol{\nabla}_I V_{e\text{-}n}(\mathbf{r}_1, \overline{\mathbf{R}}_I) \cdot \boldsymbol{\xi}_{I\lambda}. \tag{18}$$

Thanks to Eqs. (16)–(18) we can finally Taylor expand $\hat{H}$:

$$\begin{aligned} \hat{H} = &\sum_i \epsilon_i \hat{c}_i^\dagger \hat{c}_i + \hat{H}_{e\text{-}e} \\ &+ \sum_\lambda \left[\frac{\omega_\lambda}{2} \sum_s (\hat{\phi}_{s\lambda}^\dagger \hat{\phi}_{s\lambda}) + \left(\Xi_\lambda + \sum_{ij} g_{ij}^\lambda \hat{\rho}_{ij} \right) \hat{\phi}_{+\lambda} \right] \\ &+ \sum_{\lambda\lambda'} \left(\sum_{ij} \theta_{ij}^{\lambda\lambda'} \hat{\rho}_{ij} + \Theta_{\lambda\lambda'} \right) \hat{\phi}_{+\lambda} \hat{\phi}_{+\lambda'} - \hat{H}_{\text{ref}}. \end{aligned} \tag{19}$$

Equation (19) is the complete form of the quantized electron-phonon Hamiltonian. I have introduced the electronic density matrix operator: $\hat{\rho}_{ij} = \hat{c}_i^\dagger \hat{c}_j$. The different interaction potentials introduced in Eq. (19) are

$$g_{ij}^\lambda = \langle i| g^\lambda(\mathbf{r}) |j\rangle, \tag{20a}$$

$$\Xi_\lambda = \frac{1}{2} \sum_{I,J}' \partial_\lambda V_{n\text{-}n}(\overline{\mathbf{R}}_I, \overline{\mathbf{R}}_J), \tag{20b}$$

$$\theta_{nm\mathbf{k}}^{\lambda\lambda'} = \frac{1}{2} \sum_I \langle i| \partial_{\lambda\lambda'}^2 V_{e\text{-}n}(\mathbf{r}, \overline{\mathbf{R}}_I) |j\rangle, \tag{20c}$$

---
[1] I assume here to consider an extended system.

and

$$\Theta_{\lambda\lambda'} = \frac{1}{2} \left[\sum_{I,J}' \partial_{\lambda\lambda'}^2 V_{n\text{-}n}(\overline{\mathbf{R}}_I, \overline{\mathbf{R}}_J) - \delta_{\lambda\lambda'} \omega_\lambda \right]. \tag{20d}$$

In Eq. (20) the definition of the derivative along the phonon λ easily follows from Eq. (14a).

In the case of $\theta_{ij}^{\lambda\lambda'}$ it is convenient to introduce the corresponding real-space function

$$\theta_{\lambda\lambda'}(\mathbf{r}) = \frac{1}{2} \sum_I \partial_{\lambda\lambda'}^2 V_{e\text{-}n}(\mathbf{r}, \overline{\mathbf{R}}_I). \tag{21}$$

A. Reference atomic force and self-energy

I can now inspect the physical meaning of the different potentials appearing in Eq. (19) in order to arrive to a more compact form. Indeed, we start by observing that

$$\begin{aligned} \Xi_\lambda + \sum_{ij} g_{ij}^\lambda \langle \hat{\rho}_{ij} \rangle = &\frac{1}{2} \sum_{I,J} \overline{\partial_\lambda V_{n\text{-}n}(\mathbf{R}_I, \mathbf{R}_J)} \\ &+ \sum_I \int d\mathbf{r} \, \overline{\partial_\lambda V_{e\text{-}n}(\mathbf{r}, \mathbf{R}_I)}\rho(\mathbf{r}) = -F_\lambda. \end{aligned} \tag{22}$$

F_λ is the force acting on the atoms along the λ phonon direction. Equation (22) makes clear that F_λ is a functional of the electronic density $\rho(\mathbf{r})$. Equation (22) mathematically defines the equilibrium condition for the *ab initio* Hamiltonian (19): The atomic positions $\overline{\mathbf{R}}_I$ correspond to an equilibrium configuration if the corresponding electronic density is such that $F_\lambda = 0$. We will see in Sec. VI the implications of using, as reference, the results of a DFPT calculation.

The second term is

$$\begin{aligned} &\sum_{ij} \theta_{ij}^{\lambda\lambda'} \langle \hat{\rho}_{ij} \rangle + \Theta_{\lambda\lambda'} - \delta_{\lambda\lambda'} \frac{\omega_\lambda}{2} \\ &= \frac{1}{2} \left[\sum_I \int d\mathbf{r} \, \overline{\partial_{\lambda\lambda'}^2 V_{e\text{-}n}(\mathbf{r}, \mathbf{R}_I)}\rho(\mathbf{r}) \right. \\ &\quad \left. + \sum_{I,J} \overline{\partial_{\lambda\lambda'}^2 V_{n\text{-}n}(\mathbf{R}_I, \mathbf{R}_J)} - \delta_{\lambda\lambda'} \omega_\lambda \right] = -\frac{1}{2} C_{\lambda\lambda'}^{\text{ref}}. \tag{23} \end{aligned}$$

Equation (23) demonstrates that C^{ref} corresponds to the *e-n* contribution to the dynamical matrix when the atoms sit in their reference configuration.

Thanks to Eqs. (22) and (23) we obtain that

$$\begin{aligned} \hat{H} = &\sum_i \epsilon_i \hat{c}_i^\dagger \hat{c}_i + \hat{H}_{e\text{-}e} + \sum_\lambda \left[\frac{\omega_\lambda}{2} \sum_s (\hat{\phi}_{s\lambda}^\dagger \hat{\phi}_{s\lambda}) \right. \\ &+ \left. \left(\hat{\mathcal{L}}_\lambda + \sum_\mu \hat{\mathcal{Q}}_{\mu\lambda} \hat{\phi}_{+\mu} \right) \hat{\phi}_{+\lambda} \right], \end{aligned} \tag{24}$$

where

$$\hat{\mathcal{L}}_\lambda = \sum_{ij} g_{ij}^\lambda \Delta \hat{\rho}_{ij} - F_\lambda, \tag{25a}$$

$$\hat{\mathcal{Q}}_{\lambda\mu} = \sum_{ij} \theta_{ij}^{\lambda\mu} \Delta \hat{\rho}_{ij} - \frac{1}{2} C_{\lambda\mu}^{\text{ref}}, \tag{25b}$$

and $\Delta \hat{\rho}_{ij} = \hat{\rho}_{ij} - \langle \hat{\rho}_{ij} \rangle$.

Let us keep in mind that Eq. (25) can be equivalently expressed in terms of $\hat{\rho}(\mathbf{r})$:

$$\hat{\mathcal{L}}_\lambda = \int d\mathbf{r}\, g^\lambda(\mathbf{r}) \Delta\hat{\rho}(\mathbf{r}) - F_\lambda, \qquad (26a)$$

$$\hat{\mathcal{Q}}_{\lambda\mu} = \int d\mathbf{r}\, \theta^{\lambda\mu}(\mathbf{r}) \Delta\hat{\rho}(\mathbf{r}) - \frac{1}{2} C_{\lambda\mu}^{\text{ref}}. \qquad (26b)$$

III. REVIEW OF THE MANY-BODY PERTURBATION THEORY APPROACH TO THE PHONON PROBLEM

In this section I review the basic steps in the derivation of the MBPT phonon self-energy by using as a starting point the bare and undressed Hamiltonian (19). I will extend the derivation presented in Marini and Pavlyukh [16] by introducing the reference potentials defined in Sec. II A and, also, by deriving the usual second-order differential equation for the displacement-displacement Green's function from the first-order 2×2 equation of motion. Everything is derived by using the Keldysh formalism [14] and the functional derivatives method [2,47] which is an approach alternative to the standard diagrammatic method.

A. Equation of motion for the phonon displacement and momentum fields

In order to define the phonon propagator and derive its equation of motion I need as input the equations of motions for the elemental fields $\hat{\phi}_{s\lambda}$. First I switch to the time-dependent Heisenberg operatorial representation with time arguments z on the Keldysh contour [14]. The Keldysh formalism ensures that the present results are not limited to the equilibrium and/or zero-temperature cases.

I now apply Heisenberg's equation of motion (EOM) for operators,

$$\frac{d}{dz}\hat{O}(z) = i[\hat{O}(z), \hat{H}(z)]_-. \qquad (27)$$

By using the fact that

$$[\hat{\phi}_{s\lambda}, \hat{\phi}_{s'\mu}]_- = [\underline{\sigma}_2]_{ss'} s \delta_{\lambda\mu}, \qquad (28a)$$

$$[\hat{c}_i, \hat{c}_j]_+ = \hat{c}_i \hat{c}_j + \hat{c}_j \hat{c}_i = \delta_{ij}, \qquad (28b)$$

it follows that

$$\frac{d}{dz}\hat{\phi}_{-\lambda}(z) = -\omega_\lambda \hat{\phi}_{+\lambda}(z) - \hat{\mathcal{L}}_\lambda(z) - 2\sum_\mu \hat{\mathcal{Q}}_{\lambda\mu}\hat{\phi}_{+\mu}(z), \qquad (29a)$$

$$\frac{d}{dz}\hat{\phi}_{+\lambda}(z) = \omega_\lambda \hat{\phi}_{-\lambda}(z). \qquad (29b)$$

In Eq. (28), $\underline{\sigma}_2$ is the 2×2 Pauli matrix

$$\underline{\sigma}_2 = \begin{pmatrix} 0 & -i \\ i & 0 \end{pmatrix}. \qquad (30)$$

B. Phonon propagator matrix

Having then obtained the coupled EOMs for the $\hat{\phi}_{s\lambda}$ fields, we combine them to arrive at the EOM for the phonon Green's function (GF) matrix $D_{\lambda_1\lambda_2}^{s_1 s_2}(z_1, z_2)$:

$$D_{\lambda_1\lambda_2}^{s_1 s_2}(z_1, z_2) = (-i)\langle\mathcal{T}\{\Delta\hat{\phi}_{s_1\lambda_1}(z_1)\Delta\hat{\phi}_{s_2\lambda_2}^\dagger(z_2)\}\rangle, \qquad (31)$$

where $\langle\ldots\rangle$ is the trace over the exact density matrix, $\mathcal{T}$ the contour-ordering operator, and $\Delta\hat{\phi}_{s\lambda} = \hat{\phi}_{s\lambda} - \langle\hat{\phi}_{s\lambda}\rangle$. The electronic GF is

$$G(1, 2) = (-i)\langle\mathcal{T}\{\hat{\psi}(1)\hat{\psi}^\dagger(2)\}\rangle, \qquad (32)$$

with $1 = (\mathbf{r}_1, z_1)$.

The phonon GF (and self-energy) can be represented as 2×2 matrices $\underline{D}_{\lambda_1\lambda_2}(z_1, z_2)$. Its EOM can be obtained by introducing a fictitious time dependence in H, as described in Ref. [16]:

$$\hat{H}_{\xi\eta}(z) = \hat{H} + \sum_{s\lambda}\xi_{s\lambda}(z)\hat{\phi}_{s\lambda} + \int d\mathbf{r}_1 \eta(1)\hat{\rho}(\mathbf{r}_1). \qquad (33)$$

Thanks to the introduction of $\xi_{s\lambda}(z)$ it is straightforward to demonstrate that

$$D_{\lambda_1\lambda_2}^{s_1 s_2}(z_1, z_2) = \frac{\delta\langle\hat{\phi}_{s_1\lambda_1}(z_1)\rangle}{\delta\xi_{s_2\lambda_2}(z_2)}. \qquad (34)$$

In Eq. (34) the average is evaluated using $\hat{H}_{\xi\eta}(z)$. In the following all averages are dependent on ξ and η and the limit $\eta, \xi \to 0$ will be performed at the end of the derivation.

From Eqs. (34) and (29) it follows that

$$i\frac{d}{dz_1}D_{\lambda_1\lambda_2}^{s_1 s_2}(z_1, z_2)$$
$$= [\underline{\sigma}_2(\omega_{\lambda_1}\underline{D}_{\lambda_1\lambda_2}(z_1, z_2) + \delta_{z_1 z_2}\delta_{\lambda_1\lambda_2})]_{s_1 s_2}$$
$$+ \delta_{s_1-}\frac{\delta\langle\hat{\mathcal{L}}_{\lambda_1}(z_1) + 2\sum_{\lambda_3}\hat{\mathcal{Q}}_{\lambda_1\lambda_3}(z_1)\hat{\phi}_{+\lambda_3}(z_1)\rangle}{\delta\xi_{s_2\lambda_2}(z_2)}. \qquad (35a)$$

Similarly, we can evaluate the right derivative

$$i\frac{d}{dz_2}D_{\lambda_1\lambda_2}^{s_1 s_2}(z_1, z_2)$$
$$= [(\omega_{\lambda_2}\underline{D}_{\lambda_1\lambda_2}(z_1, z_2) + \delta_{z_1 z_2}\delta_{\lambda_1\lambda_2})\underline{\sigma}_2]_{s_1 s_2}$$
$$+ \delta_{s_2-}\frac{\delta\langle\hat{\mathcal{L}}_{\lambda_2}^\dagger(z_2) + 2\sum_{\lambda_3}\hat{\mathcal{Q}}_{\lambda_2\lambda_3}^\dagger(z_2)\hat{\phi}_{+\lambda_3}(z_2)\rangle}{\delta\xi_{s_1\lambda_1}(z_1)}. \qquad (35b)$$

In Eq. (35), $\delta_{z_1 z_2} = \delta(z_1 - z_2)$. We need now to evaluate the right-hand side of Eq. (35). Let us consider Eq. (35a) as the right derivative can be similarly worked out. There are two terms:

$$\frac{\delta\langle\hat{\mathcal{L}}_{\lambda_1}(z_1)\rangle}{\delta\xi_{s_2\lambda_2}(z_2)} = \int d\mathbf{r}_1 g^{\lambda_1}(\mathbf{r}_1)\frac{\delta\langle\hat{\rho}(1)\rangle}{\delta\xi_{s_2\lambda_2}(z_2)} \qquad (36)$$

and

$$\frac{\delta\langle\hat{\mathcal{Q}}_{\lambda_1\lambda_3}(z_1)\hat{\phi}_{+\lambda_3}(z_1)\rangle}{\delta\xi_{s_2\lambda_2}(z_2)}$$
$$= -\frac{1}{2}C_{\lambda_1\lambda_3}^{\text{ref}}D_{\lambda_3\lambda_2}(z_1, z_2)$$
$$+ \int d\mathbf{r}_1 \theta^{\lambda_1\lambda_3}(\mathbf{r}_1)\frac{\delta\langle\Delta\hat{\rho}(1)\hat{\phi}_{+\lambda_3}(z_1)\rangle}{\delta\xi_{s_2\lambda_2}(z_2)}. \qquad (37)$$

In evaluating Eq. (36), I have used Eq. (25a) and the fact that $\frac{\delta \Xi}{\delta \xi} = 0$. Moreover, the last term on the right-hand side of Eq. (37) is, at least, proportional to $\hat{u}_\lambda^2$ via θ. This implies that, within the harmonic approximation

$$\frac{\delta \langle \hat{\mathcal{Q}}_{\lambda_1 \lambda_3}(z_1) \hat{\phi}_{+\lambda_3}(z_1) \rangle}{\delta \xi_{s_2 \lambda_2}(z_2)} \approx -\frac{1}{2} C_{\lambda_1 \lambda_3}^{\text{ref}} D_{\lambda_3 \lambda_2}^{+s_2}(z_1, z_2). \quad (38)$$

C. Vertex function

In order to write Eq. (36) in terms of Green's functions I use the chain rule

$$\frac{\delta \langle \hat{\rho}(1) \rangle}{\delta \xi_{s_2 \lambda_2}(z_2)} = -\int d34 G(1, 3) \frac{\delta G^{-1}(3, 4)}{\delta \xi_{s_2 \lambda_2}(z_2)} G(4, 1). \quad (39)$$

The Dyson equation for the electronic Green's function is

$$G(1, 2) = G^0(1, 2) + \int d34 G^0(1, 3)$$
$$\times [V_{\text{tot}}(3) \delta_{34} + M(3, 4)] G(4, 2), \quad (40)$$

with $V_{\text{tot}}(1) = V_H(1) + \eta(1) + U(1)$ and

$$\delta_{12} = \delta_{z_1 z_2} \delta_{\mathbf{r}_1 \mathbf{r}_2} = \delta(z_1 - z_2) \delta(\mathbf{r}_1 - \mathbf{r}_2). \quad (41)$$

In Eq. (40)

$$V_H(1) = \int d\mathbf{r}_2 v(\mathbf{r}_1 - \mathbf{r}_2) \rho(2), \quad (42a)$$

$$U(1) = \sum_{\lambda_1 \lambda_2} g^{\lambda_1}(\mathbf{r}_1) \int dz_2 D_{\lambda_1 \lambda_2}^{+s_2}(z_1, z_2) \xi_{s_2 \lambda_2}(z_2). \quad (42b)$$

V_H and U are the mean field electronic potentials induced by the *e-e* (Hartree) and *e-p* (tadpole) interactions.

The mass operator appearing in Eq. (40) will not be discussed here. I assume it to be the exact $M(1, 2)$. More information can be found, for example, in Refs. [2,16].

I can now work out the functional derivative $\frac{\delta}{\delta \xi}$:

$$\frac{\delta}{\delta \xi_{s_2 \lambda_2}(z_2)} = \int d34 \frac{\delta U(3)}{\xi_{s_2 \lambda_2}(z_2)} \frac{\delta V_{\text{tot}}(4)}{\delta U(3)} \frac{\delta}{\delta V_{\text{tot}}(4)}. \quad (43)$$

I now observe that from Eq. (42b) it follows

$$\frac{\delta U(3)}{\delta \xi_{s_2 \lambda_2}(z_2)} = \sum_{\lambda_3} g^{\lambda_3}(\mathbf{r}_3) D_{\lambda_3 \lambda_2}^{+s_2}(z_3, z_2), \quad (44)$$

while

$$\frac{\delta V_{\text{tot}}(4)}{\delta U(3)} = \delta_{43} + \int d5 v(4, 5) \frac{\delta \rho(5)}{\delta U(3)}$$
$$= \delta_{43} + \int d5 v(4, 5) \chi(5, 3) = \epsilon^{-1}(4, 3). \quad (45)$$

Thanks to Eqs. (42)–(45) I can finally introduce the reducible and irreducible *e-p* vertex functions

$$\Gamma^{s_3 \lambda_3}(12, z_3) \equiv -\frac{\delta G^{-1}(1, 2)}{\delta \xi_{s_3 \lambda_3}(z_3)}, \quad (46a)$$

$$\tilde{\Gamma}(12, 3) \equiv -\frac{\delta G^{-1}(1, 2)}{\delta V_{\text{tot}}(3)}. \quad (46b)$$

The two vertex functions are connected via Eq. (43):

$$\Gamma^{s_3 \lambda_3}(12, z_3) = \sum_{\lambda_4} \int d45 \tilde{\Gamma}(12, 5)$$
$$\times \epsilon^{-1}(5, 4) g^{\lambda_4}(\mathbf{r}_4) D_{\lambda_4 \lambda_3}^{+s_3}(z_4, z_3). \quad (47)$$

Equation (47) allows me to introduce the nonlocal and time-dependent effective *e-p* interaction potential

$$\mathcal{G}^\lambda(1, z_2) = \int d\mathbf{r}_2 \epsilon^{-1}(1, 2) g^{\lambda_1}(\mathbf{r}_2). \quad (48)$$

Before connecting the vertex function to the phonon self-energy we need to derive its equation of motion. This has been already done in Ref. [16] for the reducible Γ. A similar procedure, based on the chain rule, can be followed for the irreducible $\tilde{\Gamma}$:

$$\tilde{\Gamma}(12, 3) = \delta_{12} \delta_{13} + \int d4567 \frac{\delta_t M(1, 2)}{\delta_t G(4, 5)}$$
$$\times G(4, 6) G(7, 5) \tilde{\Gamma}(67, 3). \quad (49)$$

To conclude this section we have to put together the results of Eqs. (39) and (44)–(47) to get

$$\frac{\delta \langle \hat{\mathcal{L}}_{\lambda_1}(z_1) \rangle}{\delta \xi_{s_2 \lambda_2}(z_2)} = \sum_{\lambda_4} \int d\mathbf{r}_1 d3 \, dz_4 [g^{\lambda_1}(\mathbf{r}_1) \tilde{\chi}(1, 3) \mathcal{G}^{\lambda_4}(3, z_4)]$$
$$\times D_{\lambda_4 \lambda_2}^{+s_2}(z_4, z_2)$$
$$(50a)$$

with

$$\tilde{\chi}(1, 2) = -i \int d34 G(1, 3) G(4, 1) \tilde{\Gamma}(34, 2). \quad (50b)$$

D. Equation of motion for $\underline{D}$ and the left and right self-energies

If we now use Eqs. (50) and (38) in Eq. (35) we finally arrive at the equation of motion for $\underline{D}$:

$$i \frac{d}{dz_1} \underline{D}_{\lambda_1 \lambda_2}(z_1, z_2) = \underline{\sigma}_2 (\omega_{\lambda_1} \underline{D}_{\lambda_1 \lambda_2}(z_1, z_2) + \delta_{z_1 z_2} \delta_{\lambda_1 \lambda_2})$$
$$+ \underline{I}_{\lambda_1 \lambda_2}(z_1, z_2)|_L \quad (51a)$$

and

$$-i \frac{d}{dz_2} \underline{D}_{\lambda_1 \lambda_2}(z_1, z_2) = (\omega_{\lambda_2} \underline{D}_{\lambda_1 \lambda_2}(z_1, z_2) + \delta_{z_1 z_2} \delta_{\lambda_1 \lambda_2}) \underline{\sigma}_2$$
$$+ \underline{I}_{\lambda_1 \lambda_2}(z_1, z_2)|_R, \quad (51b)$$

where

$$\underline{I}_{\lambda_1 \lambda_2}(z_1, z_2)|_L = -i \int dz_3 \sum_{\lambda_3} (\Pi_{\lambda_1 \lambda_3}^L(z_1, z_3) - C_{\lambda_1 \lambda_3}^{\text{ref}} \delta_{z_1 z_3})$$
$$\times \begin{pmatrix} D_{\lambda_3 \lambda_2}^{+-}(z_3, z_2) & D_{\lambda_3 \lambda_2}^{++}(z_3, z_2) \\ 0 & 0 \end{pmatrix} \quad (52a)$$

and

$$\underline{I}_{\lambda_1 \lambda_2}(z_1, z_2)|_R = i \int dz_3 \sum_{\lambda_3} \begin{pmatrix} D_{\lambda_1 \lambda_3}^{-+}(z_1, z_3) & 0 \\ D_{\lambda_1 \lambda_3}^{++}(z_1, z_3) & 0 \end{pmatrix}$$
$$\times (\Pi_{\lambda_3 \lambda_2}^R(z_3, z_2) - C_{\lambda_3 \lambda_2}^{\text{ref}} \delta_{z_3 z_2}). \quad (52b)$$

(a)   vertices: $\times = \mathbf{r}_1$ $\bigcirc = z_1$ $\otimes = (\mathbf{r}_1, z_1)$

(b) $g^\lambda(\mathbf{r}_1) = \boxtimes_1^\lambda$

(c) $\mathcal{G}^\lambda(\mathbf{r}_1) = \boxtimes_1^\lambda$

(d) $G(1,2) = \underset{1}{\otimes} \longleftarrow \underset{2}{\otimes}$
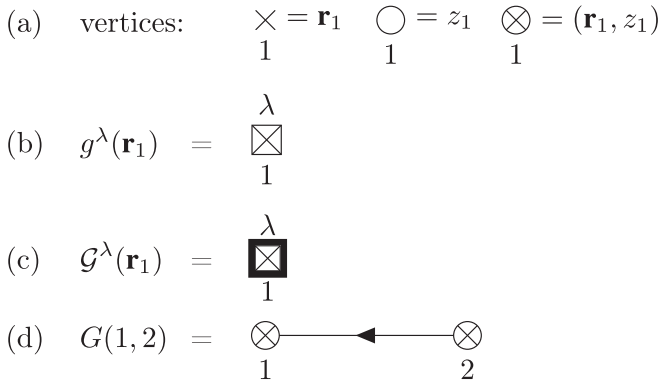
FIG. 1. Definition of the diagrammatic elements used in this work. (a) $\bigcirc$ and $\times$ represent a generic time and position point, respectively. These two symbols can be combined to indicate a time and position vertex $\oplus_1$ equivalent to $1 = (\mathbf{r}_1, z_1)$. (b) A box around a spatial point represents the *e-p* bare potential $g^\lambda(\mathbf{r}_1)$. (c) Dressed *e-p* potential. (d) Electronic Green's function.

The key ingredients in Eqs. (51) and (52) are the phonon self-energies, defined as

$$\Pi^L_{\lambda_1\lambda_2}(z_1, z_2) = \int d\mathbf{r}_1 d3 \, g^{\lambda_1}(\mathbf{r}_1) \tilde{\chi}(1,3) \mathcal{G}^{\lambda_2}(3, z_2) \quad (53a)$$

and

$$\Pi^R_{\lambda_1\lambda_2}(z_1, z_2) = \int d\mathbf{r}_2 d3 \, \mathcal{G}^{\lambda_1}(z_1, 3) \tilde{\chi}(3,2) g^{\lambda_2}(\mathbf{r}_2). \quad (53b)$$

In the following I will use the short notation $\Delta\Pi^{L/R}_{\lambda_1\lambda_2}(z_1, z_2) = \Pi^{L/R}_{\lambda_1\lambda_2}(z_1, z_2) - C^{\text{ref}}_{\lambda_1\lambda_2}\delta_{z_1z_2}$.

Equations (51)–(53) represent a crucial result of this work. It demonstrates that, if the MBPT derivation is done starting from an *ab initio* Hamiltonian, the reference atomic positions that define the zeroth order of the harmonic expansion define a term $\underline{C}^{\text{ref}}$ that needs to be removed from the full MBPT self-energy in order to avoid double counting of correlation effects. This represents the analogous of the electronic case where it is well established that the DFT exchange-correlation potential V_{xc} must be removed from the MBPT electronic self-energy [48]. Π^{ref} plays exactly the same role of V_{xc}.

Let me conclude this section by introducing the diagrammatic representation of Eq. (53a). In Fig. 1 all ingredients of the diagrammatic representation are showed and in the upper frame of Fig. 2, $\Pi^L_{\lambda_1\lambda_2}(z_1, z_2)$ is diagrammatically represented. In the lower frame of Fig. 2, instead, I show the self-energy in the random-phase approximation (RPA) that I will discuss in detail in the next sections.

IV. EQUILIBRIUM REGIME

Equations (51)–(53) are written on the Keldysh contour and, in addition, are first-order time derivatives. In this section I will demonstrate how to move in the equilibrium regime
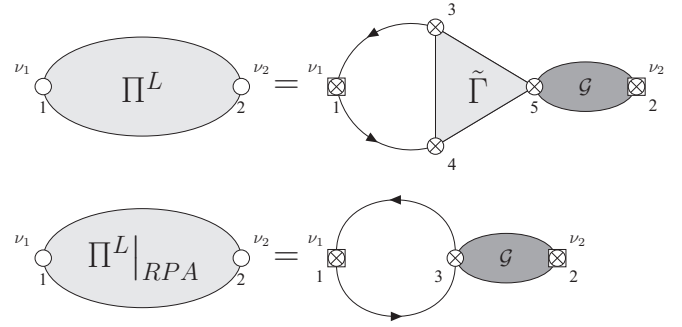
FIG. 2. Diagrammatic representation of $\Pi^L_{\lambda_1\lambda_2}(z_1, z_2)$. Full self-energy (upper frame) and within the RPA approximation corresponding to the approximation $\tilde{\Gamma} = 1$ (lower frame).

defining the corresponding self-energy for the displacement-displacement component of the phonon Green's function matrix.

As a first step we remind that the real-time components of the Green's function are obtained by applying the Langreth rules [14]. Here I am interested in the retarded component of $\underline{D}$ that I will refer to as $\underline{\mathcal{D}}(t_1, t_2)$. $\mathcal{D}$ will in general depend on t_1 and t_2 and not on $t_1 - t_2$. In order to introduce the equilibrium regime we move from

$$(t_1, t_2) \Rightarrow \left(T = \frac{(t_1 + t_2)}{2}, \tau = \frac{(t_1 - t_2)}{2} \right). \quad (54)$$

In the (T, τ) basis the equilibrium regime is defined by the condition $\frac{d}{dT}\underline{\mathcal{D}}_{\lambda_1\lambda_2}(T, \tau)|_{eq} = 0$. It follows that

$$\underline{D}_{\lambda_1\lambda_2}(t_1, t_2)\big|_{eq} = \underline{D}_{\lambda_1\lambda_2}(t_1 - t_2). \quad (55)$$

The goal now is to derive from Eqs. (51)–(53) the equation of motion for $\underline{\mathcal{D}}_{\lambda_1\lambda_2}(\tau)$. In the following I will demonstrate that the EOM for $\underline{D}_{\lambda_1\lambda_2}$ can be closed in three equivalent formulations in the subspace of $D^{++}_{\lambda_1\lambda_2}(\tau)$ only. Only one of these will lead to a symmetrized form suitable to take the static screening limit.

Let us start by the (s_1, s_2) components of Eqs. (51) and (52). The components of the left and right time derivatives are derived in Appendix A. I now define a symmetric differential operator:

$$\frac{d}{d\tau} = \frac{1}{2}\left(\frac{d}{dt_1} - \frac{d}{dt_2} \right). \quad (56)$$

From Eqs. (A1) and (A2) it follows that

$$\frac{d}{d\tau}\mathcal{D}^{++}_{\lambda_1\lambda_2}(\tau) = \frac{\omega_{\lambda_1}}{2}\mathcal{D}^{-+}_{\lambda_1\lambda_2}(\tau) - \frac{\omega_{\lambda_2}}{2}\mathcal{D}^{+-}_{\lambda_1\lambda_2}(\tau). \quad (57)$$

From Eqs. (A1b)–(A1c) and (A2b)–(A2c) we see that if we apply $\frac{d}{d\tau}$ again to Eq. (57) we can rewrite the right-hand side in terms of $\mathcal{D}^{++}$ and $\mathcal{D}^{--}$. Indeed,

$$\frac{d^2}{d\tau^2}\mathcal{D}^{++}_{\lambda_1\lambda_2}(\tau) = -\mathcal{D}^{++}_{\lambda_1\lambda_2}(\tau)\frac{(\omega^2_{\lambda_1} + \omega^2_{\lambda_2})}{4} - \mathcal{D}^{--}_{\lambda_1\lambda_2}(\tau)\frac{\omega_{\lambda_1}\omega_{\lambda_2}}{2}$$
$$- \delta(\tau)\frac{(\omega_{\lambda_1} + \omega_{\lambda_2})}{2} - \frac{1}{2}\int d\tau' \sum_{\lambda_3}[\omega_{\lambda_1}\Delta\Pi^L_{\lambda_1\lambda_3}(\tau - \tau')\mathcal{D}^{++}_{\lambda_3\lambda_2}(\tau') + \omega_{\lambda_2}\mathcal{D}^{++}_{\lambda_1\lambda_3}(\tau - \tau')\Delta\Pi^R_{\lambda_3\lambda_2}(\tau')]. \quad (58)$$

In Eq. (58) the last term on the right-hand side acquires a 2 prefactor due to the transformation $dt_3 \to d\tau'$. The last step we need to close Eq. (58) is to observe that if we assume that $\langle \mathcal{T}\{\hat{b}_{\lambda_1}(z_1)\hat{b}_{\lambda_2}(z_2)\}\rangle = \langle \mathcal{T}\{\hat{b}^\dagger_{\lambda_1}(z_1)\hat{b}^\dagger_{\lambda_2}(z_2)\}\rangle = 0$ it follows from Eq. (31) that

$$\mathcal{D}^{--}_{\lambda_1\lambda_2}(\tau) = \mathcal{D}^{++}_{\lambda_1\lambda_2}(\tau). \tag{59}$$

If we use Eq. (59) assuming also the $\mathcal{D}^{++}_{\lambda_1\lambda_2}(\tau) \sim \delta_{\lambda_1\lambda_2}\mathcal{D}^{++}_{\lambda_1}(\tau)$ and $\Delta\Pi^{++}_{\lambda_1\lambda_2}(\tau) \sim \delta_{\lambda_1\lambda_2}\Delta\Pi^{++}_{\lambda_1}(\tau)$ we finally rewrite Eq. (58) as

$$\frac{d^2}{d\tau^2}\mathcal{D}^{++}_{\lambda_1}(\tau) = -\omega_{\lambda_1}\delta(\tau) - \omega^2_{\lambda_1}\mathcal{D}^{++}_{\lambda_1}(\tau) - \frac{\omega_{\lambda_1}}{2}\int d\tau'\big[\Delta\Pi^L_{\lambda_1}(\tau-\tau')\mathcal{D}^{++}_{\lambda_1}(\tau') + \mathcal{D}^{++}_{\lambda_1}(\tau-\tau')\Delta\Pi^R_{\lambda_2}(\tau')\big]. \tag{60}$$

Equation (60) is another crucial result of this work. It defines a symmetric second-order equation of motion for the retarded phonon Green's function at the equilibrium where both the left and right self-energies appear. As it will be clear in the following Eq. (60) admits a well-defined and formally correct procedure to introduce the static-screening approximation.

Indeed, there are other two forms of the Dyson equation for D^{++} that can be obtained by applying $\frac{d}{dt_1}$ to Eq. (A1a) and $\frac{d}{dt_2}$ to Eq. (A2a):

$$\frac{d^2}{dt_1^2}\mathcal{D}^{++}_{\lambda_1}(t_1-t_2)$$
$$= -\omega_{\lambda_1}\delta_{t_1 t_2} - \omega^2_{\lambda_1}\mathcal{D}^{++}_{\lambda_1}(t_1-t_2)$$
$$- \int dt_3 \Delta\Pi^L_{\lambda_1}(t_1-t_3)\mathcal{D}^{++}_{\lambda_1}(t_3-t_2) \tag{61a}$$

and

$$\frac{d^2}{dt_2^2}\mathcal{D}^{++}_{\lambda_1}(t_1-t_2)$$
$$= -\omega_{\lambda_1}\delta_{t_1 t_2} - \omega^2_{\lambda_1}\mathcal{D}^{++}_{\lambda_1}(t_1-t_2)$$
$$- \int dt_3 \mathcal{D}^{++}_{\lambda_1}(t_1-t_3)\Delta\Pi^R_{\lambda_1}(t_3-t_2). \tag{61b}$$

As it will be clear in the next section, Eqs. (61) and (60) are equivalent when the exact left and right self-energies are used. But, they can lead to different results when the self-energy is approximated.

V. SCREENING, DOUBLE COUNTING, AND OVERSCREENING

Although the right and left self-energies have a different analytic structure, it is instructive to see why and how their perturbative expansion coincides. To this end the diagrammatic expansion provides an intuitive and graphical interpretation.

The inverse electronic dielectric function ϵ^{-1} is defined in Eq. (45) in terms of the reducible response function $\chi(1,2)$. The most common approximation for χ is the Hartree or RPA approximation which corresponds to assume $\tilde{\Gamma}(12,3) \approx \delta_{12}\delta_{13}$. Within the RPA approximation $\chi(1,2)$ is then written as

$$\chi(1,2) = \chi^0(1,2) + \int d34\,\chi^0(1,3)v(3,4)\chi(4,2)$$
$$= [\chi^0 + \chi^0 \otimes v \otimes \chi^0 + \cdots](1,2). \tag{62}$$

In the right-hand side of Eq. (62) I have used a compact form ($\otimes$) to represent the spatial convolutions. Within the RPA

we have that

$$\Pi^L_{\lambda_1\lambda_2}(t_1-t_2)\big|_{\text{RPA}} = \int d\mathbf{r}_2 d3\, g^{\lambda_1}(\mathbf{r}_1)\chi^0(1,3)\epsilon^{-1}(3,2)$$
$$\times \mathcal{G}^{\lambda_2}(t_2,2). \tag{63}$$

If we now use Eq. (62) to expand in powers of v Eq. (63) we get the diagrammatic representation of Fig. 3, upper frame. It is clear that at any order of the perturbative expansion we have $\Pi^R|_{\text{RPA}} = \Pi^L|_{\text{RPA}}$.

A. Statically screened eletron-nuclei interaction potential

As it will be clear in Sec. VI *ab initio* calculations can easily provide the statically screened *e-p* potential. Within the MBPT language this corresponds to the static $\mathcal{G}$ potential defined as

$$\mathcal{G}^\lambda(1,t_2) \approx \mathcal{G}^\lambda_S(\mathbf{r}_1) = \delta_{t_1 t_2}\int d\mathbf{r}_2\,\epsilon^{-1}(\mathbf{r}_1,\mathbf{r}_2)g^{\lambda_1}(\mathbf{r}_2). \tag{64}$$

If ϵ^{-1} is calculated by means of TD-DFT it is possible to approximate $\mathcal{G}^\lambda_S(\mathbf{r}_1) \approx \mathcal{G}^\lambda_{\text{DFPT}}(\mathbf{r}_1)$ (see Sec. VI).

We see immediately, however, that if we apply Eq. (64) to Eq. (60), and to Eq. (61) we obtain different results. This is due to the fact that if

$$\Pi^L_{\lambda_1\lambda_2}(t_1-t_2)\big|_S = \int d\mathbf{r}_1 d\mathbf{r}_2\,\mathcal{G}^{\lambda_1}_S(\mathbf{r}_1)\tilde{\chi}(1,2)g^{\lambda_2}(\mathbf{r}_2) \tag{65a}$$

and

$$\Pi^R_{\lambda_1\lambda_2}(t_1-t_2)\big|_S = \int d\mathbf{r}_1 d\mathbf{r}_2\,g^{\lambda_1}_S(\mathbf{r}_1)\tilde{\chi}(1,2)\mathcal{G}^{\lambda_2}_S(\mathbf{r}_2), \tag{65b}$$

it easily follows that

$$\Pi^L_{\lambda_1\lambda_2}(t_1-t_2)\big|_S \neq \Pi^R_{\lambda_1\lambda_2}(t_1-t_2)\big|_S. \tag{66}$$

More importantly, Eq. (65) defines self-energies that are not symmetric under $t_1 \leftrightarrow t_2$. This breakdown of the time-inversion symmetry is inconsistent with the equilibrium regime where the dynamics is invariant under a fixed-time translation. As a consequence, for example, $\Pi^{L/R}_{\lambda_1\lambda_2}(t_1-t_2)|_S$ does not respect the fluctuation-dissipation theorem (FDT) [14] that, at the equilibrium, reads as

$$\Pi^{L/R}_{\lambda_1\lambda_2}(\omega) = -\frac{1}{\pi}\int d\omega'\frac{\text{Im}\big[\Pi^{L/R}_{\lambda_1\lambda_2}(\omega')\big]}{\omega + i0^+ - \omega'}. \tag{67}$$

Equation (67) allows, for example, to identify the phonon widths with the Im[Π]. This implies that $\Pi^{L/R}_{\lambda_1\lambda_2}(t_1-t_2)|_S$ are nonphysical and cannot be used.
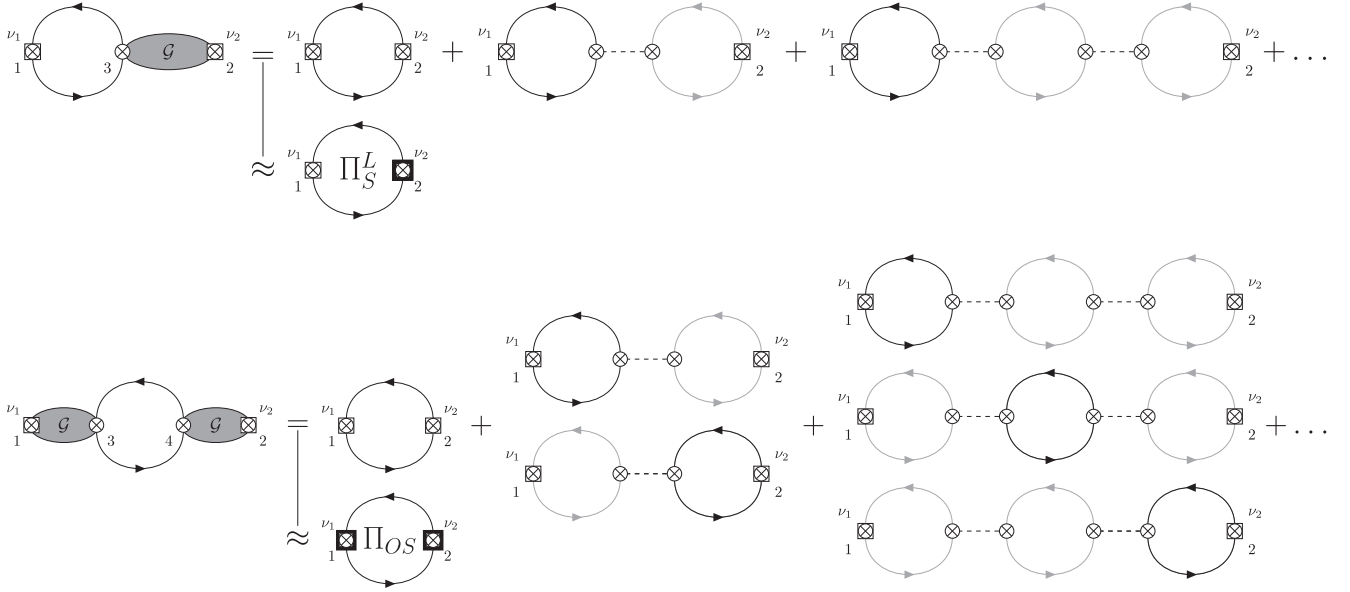
FIG. 3. Diagrammatic representation of the phonon self-energy within the random-phase approximation. At the nth order of the perturbative expansion $\Pi^L|_S$ (upper frame) contains one diagram, while $\Pi|_{OS}$ (lower frame) contains $n+1$ diagrams. The n additional diagrams in the overscreened case overcount the screening diagrams of the e-p interaction potential.

Equation (60), instead, provides a symmetric form of the self-energy suitable to take the static limit:

$$\Pi_{\lambda_1\lambda_2}(t_1 - t_2)|_S = \frac{1}{2}\big[\Pi^L_{\lambda_1\lambda_2}(t_1 - t_2)|_S + \Pi^R_{\lambda_1\lambda_2}(t_1 - t_2)|_S\big]. \tag{68}$$

Equation (68) is symmetric under $t_1 \leftrightarrow t_2$ and respect the FDT, Eq. (67).

As explained in Sec. I B several works, instead of using Eq. (68), have adopted an *overscreened* (OS) approximation

$$\Pi_{\lambda_1\lambda_2}(t_1 - t_2)|_{OS} = \int d\mathbf{r}_1 d\mathbf{r}_2 \mathcal{G}^{\lambda_1}_S(\mathbf{r}_1) \tilde{\chi}(1,2) \mathcal{G}^{\lambda_2}_S(\mathbf{r}_2). \tag{69}$$

Equation (69) *is not* compliant with the Hamiltonian (19). Indeed, it can be formally derived only by assuming

$$\widehat{H}_{e\text{-}e} = 0, \tag{70a}$$

$$g^{\lambda}(\mathbf{r}) \Rightarrow \mathcal{G}^{\lambda}_S(\mathbf{r}). \tag{70b}$$

From Eqs. (69) and (70) follow a series of observations:

(i) Eq. (70a) is not consistent with the original Hamiltonian and, consequently, the Hamiltonian that produces $\Pi|_{OS}$ does not correspond to a physical Taylor expansion of an *ab initio* Hamiltonian.

(ii) Eq. (69) is not consistent with the adiabatic limit, defined by the reference C^{ref} [Eq. (23)]. In C^{ref} only one potential $V_{e\text{-}n}$ is screened, in agreement with Eq. (68).

(iii) The diagrammatic expansion of $\Pi^L|_S$ and $\Pi|_{OS}$ is shown in Fig. 3 within the RPA approximation. In the upper frame Π^L is expanded in powers of v. We see that at each order of the expansion there is only one contribution. The gray fermionic lines come from the expansion of $\mathcal{G}$. In the lower frame, instead, the same expansion is done for $\Pi|_{OS}$ and it appears that at the order n of the expansion the OS

self-energy has n equivalent diagrams instead of 1. This means that $\Pi|_{OS}$ is affected by a severe overcounting of diagrams that, physically, corresponds to an overscreening of the e-p effective potential.

B. Numerical approximations and the *ab initio* implementation

In this section I introduce a simplified form of the phonon self-energy that will be implemented in YAMBO (Appendix C) to calculate the phonon linewidths in an exactly solvable model (Sec. V C) and in a paradigmatic material (Sec. VII):

(i) I take the *Matsubara* component of the Keldysh expressions with time arguments lying on the imaginary axis.

(ii) I separate the generalized phonon and electron indices into branch/band index and momentum index: $\alpha \to \lambda\mathbf{q}$, $i \to n\mathbf{k}$, $j \to m\mathbf{k}'$.

Being at equilibrium, I switch to frequency space via Fourier transform, considering $\Pi_{\lambda\mathbf{q}}(i\omega_n)$. Here $\omega_n = (2n+1)\pi/\beta$, with n integer and β the inverse temperature, is the Matsubara imaginary frequency.

After these steps, Eq. (60) equation reduces to

$$
\begin{aligned}
\mathcal{D}^{++}_{\lambda\mathbf{q}}(i\omega_n) = {}& \mathcal{D}^{++}_{\lambda\mathbf{q}}(i\omega_n)\big|_0 \\
& + \tfrac{1}{2}\big[\mathcal{D}^{++}_{\lambda\mathbf{q}}(i\omega_n)|_0 \Delta\Pi^L_{\lambda\mathbf{q}}(i\omega_n)\mathcal{D}^{++}_{\lambda\mathbf{q}}(i\omega_n) \\
& + \mathcal{D}^{++}_{\lambda\mathbf{q}}(i\omega_n)\Delta\Pi^R_{\lambda\mathbf{q}}(i\omega_n)\mathcal{D}^{++}_{\lambda\mathbf{q}}(i\omega_n)|_0\big],
\end{aligned} \tag{71}
$$

where the free $\mathcal{D}^{++}$ is

$$\mathcal{D}^{++}_{\lambda\mathbf{q}}(i\omega)|_0 = -\frac{\Omega_{\lambda\mathbf{q}}}{\left(\omega^2 + \Omega^2_{\lambda\mathbf{q}}\right)}. \tag{72}$$

From Eq. (71) it easily follows that we can define a final Matsubara self-energy as

$$\Pi_{\lambda\mathbf{q}}(i\omega) = \tfrac{1}{2}\big[\Pi^L_{\lambda\mathbf{q}}(i\omega_n) + \Pi^R_{\lambda\mathbf{q}}(i\omega_n)\big], \tag{73}$$

so that Eq. (71) can be finally rewritten as

$$\mathcal{D}_{\lambda\mathbf{q}}^{++}(i\omega_n) = \mathcal{D}_{\lambda\mathbf{q}}^{++}(i\omega_n)|_0[1 + \Delta\Pi_{\lambda\mathbf{q}}(i\omega_n)\mathcal{D}_{\lambda\mathbf{q}}^{++}(i\omega_n)]. \quad (74)$$

Finally, I perform the Matsubara summation of the internal frequency, so that the only integration left is the one over momenta **k**. Furthermore, this latter integration is discretized as $\int d^3\mathbf{k}/\Omega_{\mathrm{BZ}} \to \sum_k/N_k$. Here, Ω_{BZ} is the reciprocal-space volume of the Brillouin zone (BZ), while N_k is the number of **k** points in a discrete mesh spanning the BZ itself. Within the RPA approximation we get

$$\Pi_{\lambda\mathbf{q}}(i\omega_n)\big|_{\mathrm{kind}} = \frac{2}{N_k}\sum_{nm\mathbf{k}} \mathcal{G}_{mn\mathbf{k}}^{\lambda\mathbf{q}}\big|_{\mathrm{kind}} \frac{f_{m\mathbf{k}-\mathbf{q}} - f_{n\mathbf{k}}}{i\omega_n + \epsilon_{m\mathbf{k}-\mathbf{q}} - \epsilon_{n\mathbf{k}}}, \quad (75)$$

with kind = (S, OS). In Eq. (73), $\varepsilon_{n\mathbf{k}}$ and $\varepsilon_{m\mathbf{k}-\mathbf{q}}$ are electronic energies, the functions $f_{m\mathbf{k}-\mathbf{q}}$ and $f_{n\mathbf{k}}$ are the temperature-dependent electronic Fermi-Dirac occupation factors, and the prefactor of 2 comes from the spin summation. We see from these equations that the overscreened and screened self-energies differ by the coupling strengths $\mathcal{G}$:

$$\mathcal{G}_{mn\mathbf{k}}^{\lambda\mathbf{q}}\big|_{\mathrm{OS}} = \big|\langle n\mathbf{k}|\,\mathcal{G}_S^{\lambda\mathbf{q}}(\mathbf{r})\,|m\mathbf{k}-\mathbf{q}\rangle\big|^2 \quad (76a)$$

and

$$\mathcal{G}_{mn\mathbf{k}}^{\lambda\mathbf{q}}\big|_S = \frac{1}{2}\Big[\langle n\mathbf{k}|\,\mathcal{G}_S^{\lambda\mathbf{q}}(\mathbf{r})\,|m\mathbf{k}-\mathbf{q}\rangle\,\langle m\mathbf{k}-\mathbf{q}|\,g^{\lambda\mathbf{q}}(\mathbf{r})\,|n\mathbf{k}\rangle$$
$$+ \langle n\mathbf{k}|\,g_S^{\lambda\mathbf{q}}(\mathbf{r})\,|m\mathbf{k}-\mathbf{q}\rangle\,\langle m\mathbf{k}-\mathbf{q}|\,\mathcal{G}^{\lambda\mathbf{q}}(\mathbf{r})\,|n\mathbf{k}\rangle\Big]. \quad (76b)$$

C. Comparison of the screened and overscreened self-energies in an exactly solvable model

In Sec. V I have discussed the analytic properties of the $\Pi|_{\mathrm{OS}}$ self-energy and I have demonstrated that it is not a real MBPT self-energy. Nevertheless, in Ref. [13], the authors stated that the overscreened approximation better accounts for the error induced by the static approximation.

In order to provide further information and solid justifications of the two approximations (OS vs S) I consider here a model e-p Hamiltonian characterized by a single phonon with energy ω_0 interacting with a gas of free electrons via a Fröhlich-type, q-dependent e-p interaction g_q. In addition to the e-p term I include the Hartree potential so to describe the dynamical screening of g_q. The model Hamiltonian describing this system is

$$\hat{H}_m = \sum_{\mathbf{k}} \epsilon_{\mathbf{k}}\hat{c}_{\mathbf{k}}^\dagger\hat{c}_{\mathbf{k}} + \sum_{\mathbf{q}}\left[\omega_0\sum_s(\hat{\phi}_{s\mathbf{q}}^\dagger\hat{\phi}_{s\mathbf{q}}) + \sqrt{2}g_q\hat{\phi}_{+\mathbf{q}}\Delta\hat{\rho}_{\mathbf{q}}\right]$$
$$+ \frac{1}{\Omega}\sum_{\mathbf{q}}\frac{4\pi}{q^2}\langle\hat{\rho}_{-\mathbf{q}}\rangle\hat{\rho}_{\mathbf{q}} \quad (77a)$$

with

$$\hat{\rho}_{\mathbf{q}} = \frac{1}{\sqrt{N}}\sum_{\mathbf{k}}\hat{c}_{\mathbf{k}}^\dagger\hat{c}_{\mathbf{k}-\mathbf{q}}. \quad (77b)$$

Following Ref. [49], I define

$$g_q^2 = \frac{\alpha}{q^2}\frac{2\pi\omega_0}{\Omega}\sqrt{\left(\frac{2\omega_0}{m^*}\right)}, \quad (77c)$$

with α the a-dimensional e-p Fröhlich constant $q = |\mathbf{q}|$ and $k = |\mathbf{k}|$. The energy levels are assumed to be $\epsilon_{\mathbf{k}} = \frac{\mathbf{k}^2}{2m^*}$ with m^* the effective mass.

As $\hat{H}_m$ contains just the Hartree interaction term the exact real-axis phonon self-energy, obtained by evaluating Eq. (75) at $i\omega_n \to \omega + i0^+$, is

$$\Pi_q(\omega) = \frac{2}{\Omega_{RL}}g_q^2\chi_q(\omega)\big|_{\mathrm{RPA}} = \frac{2}{2\Omega_{RL}}g_q\chi_q^0(\omega)\mathcal{G}_q(\omega). \quad (78)$$

Equation (78) can be calculated exactly in terms of the independent particle response function χ^0:

$$\chi_q^0(\omega) = \int d\mathbf{k}\frac{f_{\mathbf{k}-\mathbf{q}} - f_{\mathbf{k}}}{\omega + i0^+ + \epsilon_{\mathbf{k}-\mathbf{q}} - \epsilon_{\mathbf{k}}} \quad (79a)$$

and

$$\mathcal{G}_q(\omega) = g_q\epsilon_q^{-1}(\omega). \quad (79b)$$

In the present case the S and OS self-energies, Eq. (75), are

$$\Pi_q(\omega)\big|_S = \frac{2}{\Omega_{RL}}g_q\chi_q^0(\omega)\mathcal{G}_q(0), \quad (80a)$$

$$\Pi_q(\omega)\big|_{\mathrm{OS}} = \frac{2}{\Omega_{RL}}\mathcal{G}_q(0)\chi_q^0(\omega)\mathcal{G}_q(0). \quad (80b)$$

The exact $\chi_q^0(\omega)$ can be calculated analytically. The mathematical procedure is described in Appendix B and the final result is

$$\mathrm{Im}\big[\chi_q^0(\omega)\big] = -\frac{\pi^2\Omega m^*}{q}\sum_{s=\pm1}\left[\theta\left(k_F - \left|\frac{(s\omega - \epsilon_{\mathbf{q}})m^*}{q}\right|\right)\right.$$
$$\left.\times\left(k_F^2 - \left(\frac{(s\omega - \epsilon_{\mathbf{q}})m^*}{q}\right)^2\right)\right]. \quad (81)$$

The real part of $\chi_q^0(\omega)$ can be calculated by using the FDT, Eq. (67), applied to the response function

$$\chi_q^0(\omega) = -\frac{1}{\pi}\int d\omega'\frac{\mathrm{Im}\big[\chi_q^0(\omega')\big]}{\omega + i0^+ - \omega'}. \quad (82)$$

Equations (78) and (80) provide an excellent tool to test the validity of the different approximations. In order to, however, validate the model I follow the strategy of finding the values of Ω, ω_0, α, and m^* the provide the best fit of the dielectric properties of a realistic paradigmatic material MgB$_2$.

From Eq. (79b) it is evident that a key quantity that dictates most of the screening properties is the inverse dielectric function $\epsilon_q^{-1}(\omega)$. In the model Hamiltonian this is exact within the RPA approximation. In Fig. 4 the $\epsilon_q^{-1}(\omega)$ calculated in MgB$_2$ and in the model Hamiltonian are compared for several transferred momenta and in the energy range (0, 200) meV that is relevant for the phonon dynamics. The thickness of the lines is proportional to q. From the figure we see that both the imaginary part and the variation of the real part are well described. In particular, the imaginary part shows the same frequency and momentum trend of the full, *ab initio*, calculation. The parameters used are tabulated in Table I. In Fig. 5, I show the q dependency of the on-the-mass shell phonon width, defined as

$$\gamma_q = -\mathrm{Im}[\Pi_q(\omega_0)], \quad (83)$$
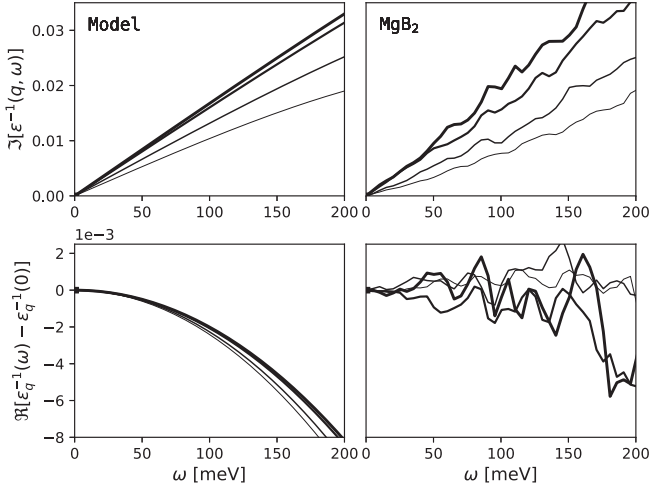
FIG. 4. Inverse dielectric function $\epsilon_q^{-1}(\omega)$ calculated analytically (left frames) and numerically in the case of MgB$_2$ (right frames) in the low-energy range relevant to the phonon dynamics. The linewidths are proportional to q and the left and right frames span the same ϵ_q^{-1} range. No rescaling has been applied. The comparison shows that the generalized Fröhlich model Hamiltonian provides an excellent description of the low-energy properties of MgB$_2$.

as function of $q - q_c$. q_c is a critical momentum under which the phonon widths are zero by construction. q_c is defined by the condition

$$\left| s\omega_0 + \frac{q_c^2}{2m^*} \right| = \frac{k_F q_c}{m^*} \quad \text{with } s = \pm 1. \tag{84}$$

Π_q is calculated exactly (solid line), via Eq. (80a) (dotted line) and via the doubly screened approximation, Eq. (80b) (dashed line). We see clearly that, while the $\Pi_q|_{\mathrm{S}}$ performs very well for all momentum range, the $\Pi_q|_{\mathrm{OS}}$ largely underestimates the exact phonon widths.

More importantly, $\Pi_q|_{\mathrm{OS}}$ shows a wrong $q \to 0$ behavior. In order to understand the origin of this we notice that $\chi_q^0(\omega) \xrightarrow[q \to 0]{} O(1)$, with the limit taken such that $\omega < k_F q$. From Eq. (78) it follows that

$$\mathcal{G}_q(0) = \frac{q^2 g_q}{q^2 - 4\pi \chi_q^0(0)} \xrightarrow[q \to 0]{} q. \tag{85}$$

If we now notice that from Eq. (81) it follows that $\mathrm{Im}[\chi_q^0(\omega)] \xrightarrow[q \to 0]{} \frac{1}{q}$ we finally obtain that

$$\Pi_q(\omega) \xrightarrow[q \to 0]{} \begin{cases} 1/q, & \text{exact} \\ 1/q, & \text{S} \\ q, & \text{OS} \end{cases} \tag{86}$$

and, indeed, in Fig. 5 $\gamma_q|_{\mathrm{OS}} \xrightarrow[q \to 0]{} q$.

TABLE I. Generalized Fröhlich Hamiltonian parameters used to reproduce the MgB$_2$ $\epsilon_q^{-1}(\omega)$. The simulation box is a cubic cell with lattice constant a.

Parameter	Value
a	20 a.u.
ω_0	100 meV
α	5
m^*	0.15 m_e
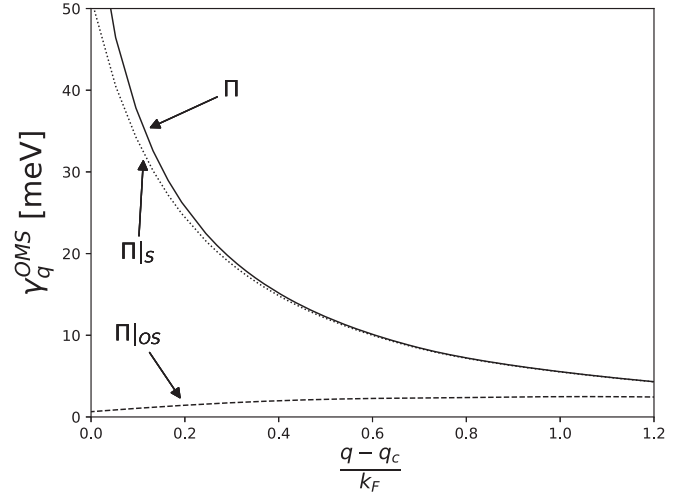
FIG. 5. Phonon widths γ_q calculated by using the exact self-energy (solid), the $\Pi|_{\mathrm{S}}$ (dotted), and the $\Pi|_{\mathrm{OS}}$ (dashed). The overscreened OS approximation largely underestimates the exact self-energy and shows a wrong long-range, $q \to 0$, behavior. The momentum range starts from q_c that represents the smallest momentum under which the phonon widths are zero by definition (see text).

Equation (86) and Fig. 5 represent a clear demonstration that $\Pi|_{\mathrm{OS}}$ *is not* a many-body compliant approximation and it leads to a, potentially severe, underestimation of the phonon widths.

VI. ON THE MERGING OF MBPT WITH THE CLASSICAL BORN-OPPENHEIMER APPROXIMATION

In Sec. II A I have introduced the reference system of phonons without specifying the corresponding atomic coordinates. In this section I will discuss the connection between the classical treatment of Eq. (5) and MBPT. In particular, in order to bridge the quantistic treatment with DFPT, it is essential to connect the different potentials that appear in Eq. (19) with their classical counterparts.

At this point it is essential to note that the reference BO energy surface defines only the reference dynamical matrix, Eq. (23). The residual atomic force, Eq. (22), is defined by the reference positions. In order to connect those two quantities we need to formally introduce the BO surface of Eq. (5). This is obtained by calculating the average of $\hat{H}$ without including the nuclear kinetic operator and treating the atomic position operators as classical variables:

$$\hat{H}_{\mathrm{BO}} = \hat{H}_e + \hat{H}_{n\text{-}n} + \hat{H}_{e\text{-}n}, \tag{87a}$$

$$E_{\mathrm{BO}}(\mathbf{R}) = H_{n\text{-}n}(\mathbf{R}) + \langle \hat{H}_e + \hat{H}_{e\text{-}n}(\mathbf{R}) \rangle. \tag{87b}$$

If we now select a specific set of atomic positions, $\mathbf{R}_{\mathrm{BO}}$, we can calculate the corresponding density $\rho(\mathbf{r})|_{\mathrm{BO}}$ dynamical matrix

$$\overleftrightarrow{C}_{IJ}|_{\mathrm{BO}} = \nabla_I \nabla_J E_{\mathrm{BO}}(\mathbf{R})|_{\mathbf{R}=\mathbf{R}_{\mathrm{BO}}}, \tag{88}$$

FIG. 6. Schematic representation of the connection between the classical harmonic expansion around an arbitrary set of atomic positions on the BO surface and MBPT.

and the force F_I

$$\mathbf{F}_I|_{\text{BO}} = -\nabla_I E_{\text{BO}}(\mathbf{R})|_{\mathbf{R}=\mathbf{R}_{\text{BO}}}. \tag{89}$$

For a generic atomic configuration the force can be nonzero and, as we are not in the equilibrium configuration, the phonon frequencies can even be negative. At this point we can also define the classical equilibrium condition such that $\mathbf{F}_I|_{\text{BO}} = \mathbf{0}$. These conceptual steps are schematically described in Fig. 6.

As described at length in this work the fully quantistic treatment of $\hat{H}$ implies the presence, in the e-p interaction, of a force term defined by Eq. (22). We can now connect the reference dynamical matrix and the BO by assuming

$$\overline{\mathbf{R}} = \mathbf{R}_{\text{BO}}. \tag{90}$$

It follows that

$$F_\lambda^{\text{ref}} = F_\lambda|_{\text{BO}} + \Delta F_\lambda|_{\text{MB}}, \tag{91a}$$

$$C_{\lambda\lambda'}^{\text{ref}} = C_{\lambda\lambda'}|_{\text{BO}}. \tag{91b}$$

Equation (91) is written in the BO phonon basis that, thanks to Eq. (90), corresponds to the reference phonon basis. In Eq. (91a)

$$\Delta F_\lambda|_{\text{MB}} = \sum_I \int d\mathbf{r} \, \overline{\partial_\lambda V_{e\text{-}n}(\mathbf{r}, \mathbf{R}_I)} [\rho(\mathbf{r})|_{\text{BO}} - \rho(\mathbf{r})] \tag{92}$$

Equation (92) defines the MBPT equivalent of the classical equilibrium as the atomic configuration such that the *total* force is zero.

The physical picture is that if we start from a BO atomic position, the MBPT will feel a force that will be stronger when the initial reference position is far from a BO equilibrium or there is a strong e-p interaction. In any case, even if we start from a zero classical force configuration, there will still be a residual force that is needed to move the system in the MBPT equilibrium. It is important to note, however, that if $\rho(\mathbf{r}) \sim \rho(\mathbf{r})|_{\text{BO}}$ the BO phonons will be renormalized but the equilibrium positions will not be effected.

A. Case of the density functional theory reference system

Within DFPT, atoms are treated classically and the theory is based on the BO. In practice density functional methods are *ab initio* approaches to calculate $E_{\text{BO}}(\mathbf{R})$, the atomic configuration corresponding to the equilibrium and the oscillations around this equilibrium in a fully self-consistent way and treating correlation exactly [50].

DFT and DFPT, therefore, are natural candidates to be used as reference system. In this case, by definition,

$$\mathbf{R}_{\text{BO}} = \mathbf{R}_{\text{DFPT}} \Rightarrow F_\lambda|_{\text{BO}} = 0, \tag{93}$$

and the MB correction will, eventually, move the equilibrium positions in the new configuration where also $\Delta F_\lambda|_{\text{MB}} = 0$.

In addition $\overleftrightarrow{C}_{IJ}^{\text{ref}} = \overleftrightarrow{C}_{IJ}^{\text{ref}}|_{\text{DFPT}}$, which implies that Eq. (23) reduces to

$$C_{\lambda_1\lambda_2}^{\text{ref}} = \sum_I \int d\mathbf{r} \, \overline{\partial_{\lambda_1} V_{e\text{-}n}(\mathbf{r}, \mathbf{R}_I)} \, \overline{\partial_{\lambda_2}\rho(\mathbf{r})|_{\text{DFPT}}}. \tag{94}$$

Equation (94) is a by-product of any DFPT calculation. It is interesting, however, to investigate if it is possible, and under which conditions, to connect C^{ref} to the static limit of Π, defined in Eq. (68).

The answer to this question is greatly simplified by the simple form of the exact phonon self-energy, Eq. (63), that is written in terms of the irreducible response function and dielectric function. Those two quantities can be indeed calculated by using DFT. The response function defined in Eq. (50b) includes e-e and e-n correlation effects. Indeed, also the inverse dielectric depends on the atomic fluctuations. In the electronic case this is a well-known effect that leads to the nondiagonal Debye-Waller correction [51].

If we neglect e-n effects in the response function and dielectric function we can approximate the mass operator with the the DFT exchange-correlation potential:

$$M(1, 2) \approx \delta_{12} V_{\text{xc}}(1). \tag{95}$$

Thanks to Eq. (95) we can calculate exactly all ingredients of Π by using DFT and it follows that, at the equilibrium, $\Pi_{\lambda_1\lambda_2}(\omega)$ reduces to

$$\Pi_{\lambda_1\lambda_2}(\omega) \xrightarrow[\omega\to 0]{\text{DFT}} \int d\mathbf{r}_1 d\mathbf{r}_2 g^{\lambda_1}(\mathbf{r}_1) \chi_0(\mathbf{r}_1, \mathbf{r}_2; \omega = 0)|_{\text{DFT}}$$
$$\times \mathcal{G}^{\lambda_1}(\mathbf{r}_2)|_{\text{DFT}}. \tag{96}$$

We can now notice that, thanks to Kubo,

$$\int d\mathbf{r}_2 \chi_0(\mathbf{r}_1, \mathbf{r}_2; \omega = 0)|_{\text{DFT}} \mathcal{G}^{\lambda_2}(\mathbf{r}_2)|_{\text{DFT}} = \overline{\partial_{\lambda_2}\rho(\mathbf{r}_1)|_{\text{DFPT}}}, \tag{97}$$

which leads to the final result

$$\Pi_{\lambda_1\lambda_2}(\omega)|_S \xrightarrow[\omega\to 0]{\text{DFT}} C_{\lambda_1\lambda_2}^{\text{ref}}. \tag{98}$$

Equation (98) means that if we use a mean field, DFT approximation for the electronic self-energy and, in addition, we take the static limit of all components of the phonon self-energy we obtain that the static phonon self-energy coincides with the static electron-nuclei component of the DFPT density matrix.

Another consequence of using DFT to describe the electronic linear response is that we can link the static limit of the

FIG. 7. Phonon band structure of MgB_2. The phonon mode symmetries at the A point are given. The modes and **q** regions exhibiting large coupling to the σ and π bands are emphasized in blue and red, respectively, and are analyzed in Fig. 9.

time-dependent effective *e-n* interaction potential (48) to the DFPT potential

$$\mathcal{G}^\lambda(\mathbf{r}_1)\big|_{\text{DFPT}} = \int d\mathbf{r}_2 \epsilon_{\text{DFT}}^{-1}(\mathbf{r}_1, \mathbf{r}_2) g^{\lambda_1}(\mathbf{r}_2). \quad (99)$$

$\mathcal{G}^\lambda|_{\text{DFPT}}$ is encoded in several public *ab initio* codes and it is the by-product of any DFPT phonon calculation.

At this point, it is crucial to observe that Eq. (98) does not hold for the overscreened self-energy:

$$\Pi_{\lambda_1\lambda_2}(\omega)|_{\text{OS}} \xrightarrow[\omega \to 0]{\text{DFT}} \int d\mathbf{r}_1 d\mathbf{r}_2 \mathcal{G}^{\lambda_1}(\mathbf{r}_1)$$
$$\times |_{\text{DFT}} \chi_0(\mathbf{r}_1, \mathbf{r}_2; \omega)|_{\text{DFT}} \mathcal{G}^{\lambda_1}(\mathbf{r}_2)|_{\text{DFT}} \neq C_{\lambda_1\lambda_2}^{\text{ref}}. \quad (100)$$

VII. RESULTS IN A PARADIGMATIC MATERIAL: MgB_2

Magnesium diboride, MgB_2, is a metallic layered material composed of alternating two-dimensional (2D) sheets of boron and magnesium. It transitions to phonon-mediated superconductivity at the critical temperature $T_c = 39$ K [52]. This behavior is almost entirely due to *e-p* coupling relative to the boron atoms, whose electrons form in-plane σ and out-of-plane π bonds. These bonds are in turn responsible for the existence of two superconducting band gaps, with different theoretical T_c [53–55]. I will briefly discuss the connection between phonon widths and superconductivity in Sec. VIII 2. What is relevant in the present context is that the superconductive properties of MgB_2 clearly point to a strong *e-p* coupling. In particular, the σ bands are considered to yield a giant "anomalous" *e-p* coupling due to the strong orbital overlap induced by the in-plane optical phonon mode E_{2g}, as opposed to the π bands undergoing a weak coupling. The calculated phonon dispersions are reported in Fig. 7 and the numerical details, code developments, and calculation flow are discussed in Appendix C.

The E_{2g} phonon linewidths have been extensively studied, both theoretically and experimentally, along the ΓA [25,31,34] and ΓM [56] directions in the hexagonal Bril-
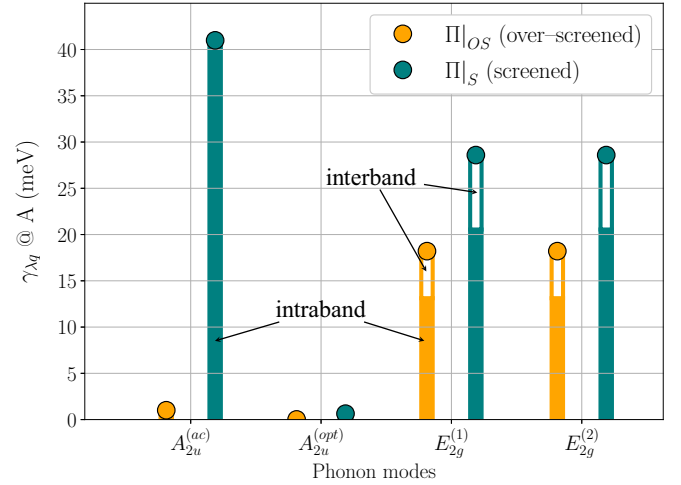
FIG. 8. Phonon linewidths in MgB_2 computed at the A point in the Brillouin zone. Only the relevant phonon modes are shown. Orange: Overscreened (Π_{OS}) linewidths. Teal: Screened (Π_{S}) linewidths. The full and empty bars represent the contributions to the linewidths stemming from intraband and interband processes, respectively.

louin zone. In these studies, the comparison is made between the full width at half-maximum of inelastic x-ray scattering spectral peaks and the phonon widths. As mentioned in the Introduction, all calculations performed so far have used the overscreened formulation, Eq. (69). The results show in general a reasonable agreement, though particularly along ΓA the experimental linewidths are found to be larger than the theoretical results. For example, in Ref. [34] a theoretical value of 20.35 meV is found at point A, while the experimental peak width is closer to 30 meV.

Let me start the discussion from the calculation of the E_{2g} mode. As can be seen from Fig. 8, I obtain 18.2 meV in the overscreened case, in very good agreement with the same calculation in Ref. [34]. The screened case, Eq. (68), gives instead the value of 28.6 meV, showing a 57% increment in the phonon linewidths. Let us notice that in the case of σ bands, around 70% of the contribution come from "intraband" terms (i.e., elecron-hole pairs are formed within the same σ subband), while the remaining 30% are due to "interband" terms involving different σ subbands. The large 57% increase in the linewidths is also the average along the full ΓA direction, as can be seen from Fig. 9(a), while a strong increase also appears along the ΓM direction. Along the latter, both overscreened and screened linewidths sensibly decrease after the midpoint from Γ to M due to a sharp increase of the relative phonon energies. The comparison with experiment is difficult due to the large error bars, but overall we do obtain a better agreement compared to the overscreening case (compare with Fig. 3 in [34] and Fig. 3 in [56] for the ΓA and ΓM directions, respectively).

The E_{2g} mode is not the only one undergoing large changes when overscreening is removed. In fact, we see from Fig. 8 that also the acoustic $A_{2u}^{(ac)}$ mode gains a giant linewidth increase from 1 meV (overscreened case) to 41 meV (screened case). By looking at Fig. 9(b) we realize that these giant linewidths appear along the full ΓA direction, where
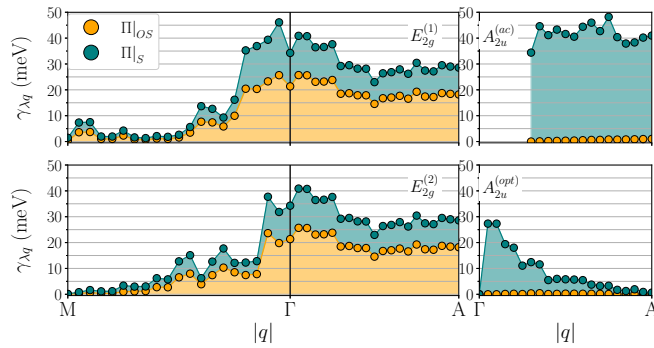
FIG. 9. Phonon linewidths of (a) the E_{2g} optical modes along the MΓA path and (b) the $A_{2u}^{(ac)}$ acoustic (top) and optical $A_{2u}^{(opt)}$ (bottom) modes along ΓA. Orange: overscreened (OE) coupling. Teal: screened (no OE) coupling.

the acoustic $A_{2u}^{(ac)}$ mode maintains an average linewidth of 42 meV, and also characterize the higher-energy, optical mode of the same symmetry. Now, the infrared-active A_{2u} modes involve out-of-plane oscillations of the boron atoms; furthermore, we see that the linewidth is composed by purely intraband, jelliumlike, contributions. As discussed in Sec. V C the OS self-energy largely underestimates the phonon widths practically for most of the $|q|$ values. This underestimation contributes to the large enhancing of the widths in the ΓA direction of MgB$_2$. Our results suggest that the π-band e-p coupling may also be anomalous.

Interestingly, the acoustic A_{2u} linewidths remain constant along ΓA despite strong variations in the relative phonon energies, while the optical A_{2u} linewidths decrease from 28 to 0.6 meV despite the phonon energies being roughly constant. We also point out that such a giant overscreening effect is not limited to the coupling with the π bands along ΓA, but also appears, although to a lesser extent, in the linewidths of the in-plane E_{1u} modes, which couple with the σ bands, along ΓM (here the largest effect is on the higher-energy acoustic E_{1u} mode up to $0.5\Gamma M$, where the screened linewidths rise to 15–20 meV).

VIII. CLOSING REMARKS

Due to the many implications of this work I conclude it by splitting the discussion in three sections. In the first (Sec. VIII 1) I will summarize the theoretical implications of using an overscreened formulation for the phonon self-energy. In the second (Sec. VIII 2) I will briefly discuss the implications, mostly conceptual, on the calculation of the Eliashberg function when it is written in terms of the phonon widths. I will then, finally, conclude with a general section of conclusions in Sec. VIII 3.

1. Summary of the evidences of an overscreening error in the phonon self-energy

One of the goals of this work is to propose a controllable approximation to the phonon self-energy Π that can be merged with DFPT making possible accurate *ab initio* calculations of phonon properties.

TABLE II. Summary of the properties of the exact phonon self-energy compared to the screened and overscreened approximations.

Self–energy	MBPT compliant Sec. V	$q \to 0$ Sec. V C	D_n Sec. V A	$\omega \to 0$ $C_{\lambda_1 \lambda_2}^{\text{ref}}$ Sec. VI A
Π	yes	$1/q$	1	yes
$\Pi\vert_S$	yes	$1/q$	1	yes
$\Pi\vert_{OS}$	no	q	n+1	no

From a general point of view any approximation to Π should be *controllable*. For *controllable* I mean that the error induced by the use of specific approximations should be estimated, even if roughly, and connected to characteristic physical properties of the materials. A family of properties that can help in defining a *controllable* approximation are the exact limits $\mathbf{q} \to 0$ and $\omega \to 0$.

In the present case I have used the following conditions to define a *controllable* approximation to Π (also tabulated in Table II):

MBPT compliant. The series of approximations used must be applied to an initial formulation that, being MBPT, admits a diagrammatic expansion. To be MBPT compliant means to respect the basic rules of the diagrammatic expansion like the fluctuation-dissipation theorem and the time-reflection symmetry. This point was studied in detail in Sec. V where I showed that the overscreened approximation overcounts bubble diagrams and, therefore, is not MBPT compliant. In practice this means that if D_n is the number of bubbles at the nth order of the diagrammatic expansion the overscreened approximation has n diagrams more compared to the screened and exact expressions (Sec. V A).

$q \to 0$ *and* $\omega \to 0$. Two very important limits that must be respected by the approximation are the static and zero momentum limits. As discussed in Sec. VI A the overscreened approximation does not reduce to the reference, adiabatic, dynamical matrix that is written in terms of a singly screened e-p potential. At the same time, the exact solution of the generalized Fröhlich Hamiltonian, discussed in Sec. V C, has demonstrated that the overscreened approximation has a wrong $q \to 0$ limit.

The conclusion of this section is, thus, that the overscreened approximation, affected by the overscreening error, is not a *controllable* and physically sound MBPT approximation.

2. Implications on the calculation of the Eliashberg function

In 1972 Allen [17] introduced a formulation of the Eliashberg function where

$$\alpha^2 F(\omega) \propto \sum_{\mathbf{q}\lambda} \gamma_{\lambda\mathbf{q}} \delta(\omega - \Omega_{\lambda\mathbf{q}}). \tag{101}$$

The basic idea of the work of Allen was to make possible to calculate the spectral function by using quantities accessible in experimental, neutron scattering, experiments.

As already noted by Allen in 1983 [20] and demonstrated here the phonon widths defined in Eq. (101) are affected by a severe overscreened error. It is important to note that the

expression of the Eliashberg function in terms of the *e-p* potential is well known and correct. The overscreening effect appears if the phonon widths are connected to $\alpha^2 F(\omega)$ via Eq. (101).

3. Conclusions

In this work I have reanalyzed the many-body description of the phonon dynamics from several aspects. I have developed a general framework to evaluate the phonon self-energy that admits a controllable static-screening approximation avoiding the overscreening error.

By reviewing and extending the literature I demonstrate that the inclusion of all *ab initio e-n* and *n-n* potentials leads to additional force and quadratic terms in the *e-p* Hamiltonian. These terms are shown to be essential in the merging of MBPT with *ab initio* density functional theories.

The equilibrium Dyson equation for the phonon displacement Green's function has been derived on the Keldysh contour and the equilibrium limit has been carefully derived. I showed that there exist three equivalent formulations in the equilibrium limit of which only one is suitable to take the static-screening approximation. This formulation allows for a formal static limit without breaking the time-reflection symmetry, needed to obtain a controllable and many-body compliant approximation.

The final, symmetric, expression of the phonon self-energy has been compared with the exact solution of a generalized Fröhlioch Hamiltonian. I showed that the overscreened approximation fails in describing the **q** exact dependence of the $\Pi_q(\omega)$ that, instead, is well described by the screened approximation proposed here.

I also provided a first-principles numerical scheme for the calculation of overscreening error-free phonon linewidths in the equilibrium case, at no additional cost with respect to the state-of-the-art, systematically overscreened approach. This can be applied to any system whose mean field description is

accessible via DFPT. The scheme is applied to MgB_2 where I demonstrate several important implications of using the proposed screened phonon self-energy.

The final results of this work lead to implications in many applications where the phonon dynamics plays a crucial role. This ranges from phonon width and energy renormalizations due to nonadiabatic effects to real-time processes as involved in thermal transport and lattice dynamics.

APPENDIX A: EXPLICIT EXPRESSION FOR THE $\mathcal{D}_{\lambda_1\lambda_2}^{s_1 s_2}(t_1 - t_2)$ EQUATIONS OF MOTION

The equation of motion for the components of the equilibrium $\underline{\mathcal{D}}$ can be found by expanding the right-hand side of Eqs. (51) and (52). For the left derivative we have

$$\frac{d}{dt_1}\mathcal{D}_{\lambda_1\lambda_2}^{--}(t_1 - t_2) = -\omega_{\lambda_1}\mathcal{D}_{\lambda_1\lambda_2}^{+-}(t_1 - t_2) - \int dt_3 \sum_{\lambda_3} \Delta\Pi_{\lambda_1\lambda_3}^{L}(t_1 - t_3)\mathcal{D}_{\lambda_3\lambda_2}^{+-}(t_3 - t_2), \tag{A1a}$$

$$\frac{d}{dt_1}\mathcal{D}_{\lambda_1\lambda_2}^{-+}(t_1 - t_2) = -\omega_{\lambda_1}\mathcal{D}_{\lambda_1\lambda_2}^{++}(t_1 - t_2) - \int dt_3 \sum_{\lambda_3} \Delta\Pi_{\lambda_1\lambda_3}^{L}(t_1 - t_3)\mathcal{D}_{\lambda_3\lambda_2}^{++}(t_3, t_2) - \delta_{t_1 t_2}, \tag{A1b}$$

$$\frac{d}{dt_1}\mathcal{D}_{\lambda_1\lambda_2}^{+-}(t_1 - t_2) = \omega_{\lambda_1}\mathcal{D}_{\lambda_1\lambda_2}^{--}(t_1 - t_2) + \delta_{t_1 t_2}, \tag{A1c}$$

$$\frac{d}{dt_1}\mathcal{D}_{\lambda_1\lambda_2}^{++}(t_1 - t_2) = \omega_{\lambda_1}\mathcal{D}_{\lambda_1\lambda_2}^{-+}(t_1 - t_2). \tag{A1d}$$

In the case of the right derivative it follows that

$$\frac{d}{dt_2}\mathcal{D}_{\lambda_1\lambda_2}^{--}(t_1 - t_2) = -\omega_{\lambda_2}\mathcal{D}_{\lambda_1\lambda_2}^{-+}(t_1 - t_2) - \int dt_3 \sum_{\lambda_3} \mathcal{D}_{\lambda_1\lambda_3}^{-+}(t_1 - t_3)\Delta\Pi_{\lambda_3\lambda_2}^{R}(t_3 - t_2), \tag{A2a}$$

$$\frac{d}{dt_2}\mathcal{D}_{\lambda_1\lambda_2}^{-+}(t_1 - t_2) = \omega_{\lambda_2}\mathcal{D}_{\lambda_1\lambda_2}^{--}(t_1 - t_2) + \delta_{t_1 t_2}, \tag{A2b}$$

$$\frac{d}{dt_1}\mathcal{D}_{\lambda_1\lambda_2}^{+-}(t_1 - t_2) = -\omega_{\lambda_2}\mathcal{D}_{\lambda_1\lambda_2}^{++}(t_1 - t_2) - \int dt_3 \sum_{\lambda_3} \mathcal{D}_{\lambda_1\lambda_3}^{++}(t_1 - t_3)\Delta\Pi_{\lambda_3\lambda_2}^{R}(t_3 - t_2) + \delta_{t_1 t_2}, \tag{A2c}$$

$$\frac{d}{dt_2}\mathcal{D}_{\lambda_1\lambda_2}^{++}(t_1 - t_2) = \omega_{\lambda_2}\mathcal{D}_{\lambda_1\lambda_2}^{+-}(t_1 - t_2). \tag{A2d}$$

APPENDIX B: EXACT INDEPENDENT PARTICLE RESPONSE FUNCTION IN THE EXTENDED FRÖHLICH HAMILTONIAN

I now consider the zero-temperature case where $f_{\mathbf{k}} = \theta(\epsilon_{\mathbf{k}} - \frac{k_F^2}{2m^*})$. This implies that the $\mathbf{k}$ summation is restricted to $|\mathbf{k}| < k_F$. We now rewrite Eq. (79a) as

$$\chi_q^0(\omega) = J_q(\omega) + J_q^*(-\omega), \quad \text{(B1a)}$$

with

$$J_q(\omega) = \int d\mathbf{k} \, f_{\mathbf{k}}(\omega + i0^+ + \epsilon_{\mathbf{k}} - \epsilon_{\mathbf{k-q}})^{-1}. \quad \text{(B1b)}$$

I now notice that if we move to spherical coordinates with the $\hat{z}$ axis along $\mathbf{q}$ we get

$$J_q(\omega) = 2\pi \int_{-1}^{1} dx \int_0^{k_F} k^2 \left(\omega - \frac{q^2}{2m^*} + \frac{kqx}{m^*} + i0^+ \right)^{-1}. \quad \text{(B2)}$$

Let us now focus on the $\text{Im}[J_q(\omega)]$. In Eq. (B2) appears $\delta(\omega - \frac{q^2}{2m^*} + \frac{kqx}{m^*})$ which implies

$$x = -\frac{(\omega - \frac{q^2}{2m^*})m^*}{kq}. \quad \text{(B3)}$$

We now distinguish two cases: $\omega = \frac{q^2}{2m^*}$ and $\omega \neq \frac{q^2}{2m^*}$.

Case I: $\omega = \frac{q^2}{2m^*}$. In this case the integral in Eq. (B2) is straightforward and gives

$$\text{Im}[J_q(\omega)]\big|_{\omega = \frac{q^2}{2m^*}} = -\frac{\pi^2 m^* k_F^2}{q}. \quad \text{(B4)}$$

Case II: $\omega \neq \frac{q^2}{2m^*}$. In this case the k range in Eq. (B2) is $k \in [k_0, k_F]$ with

$$k_0 = \left| \omega - \frac{q^2}{2m^*} \right| \frac{m^*}{q}. \quad \text{(B5)}$$

The integral in Eq. (B2) reduces to

$$\text{Im}[J_q(\omega)]\big|_{\omega \neq \frac{q^2}{2m^*}} = -\frac{\pi^2 m^*}{q} \left(k_F^2 - k_0^2 \right) \theta(k_F - k_0). \quad \text{(B6)}$$

By using Eqs. (B4) and (B6) in Eq. (B1) we finally obtain Eq. (81).

APPENDIX C: CODE DEVELOPMENT

The codes used for the implementation of this work and the subsequent numerical calculations were QUANTUM ESPRESSO (QE) [58] for the DFT and DFPT steps, and YAMBO [59] for the calculation of the phonon linewidths. Below I discuss the code implementation that was necessary to compute the equilibrium phonon self-energy, and next the general scheme of a linewidth calculation.

1. QUANTUM ESPRESSO

The bare electron-phonon matrix elements $g_{mnk}^{\lambda q}$ [Eq. (14a)] were extracted from a QE-DFPT calculation by modifying the part relative to the ph.x executable and in particular the sub-routines contained in /PHonon/PH/elphon.f90 so that the

bare matrix elements could be stored and printed in a format readable by YAMBO. The modifications were done on version 6.6 of the QE distribution [60]. Note that the (complex) spatially integrated matrix elements of the (real) variation of the bare e-p interaction are directly extracted.

2. YAMBO

Equations (68) and (69) were implemented in YAMBO, version 5.0 [61], as part of the "phonon" project relative to the yambo_ph executable. The implementation is fully parallel.

Since Eqs. (68) and (69) require a very large $\mathbf{k}$-point mesh in reciprocal space to be accurately converged, a double-grid support was added in order to compute electronic eigenvalues on a finer grid with respect to the one used for the e-p calculations. Let me denote the fine grid as FG and the original, coarse grid as CG. From now on, reciprocal-space points belonging to the FG (CG) are written as lowercase $\mathbf{k}$ (uppercase $\mathbf{K}$).

Let us start rewriting Eq. (75) for a $\mathbf{Q}$ point in the CG as

$$\Pi_{\lambda\mathbf{Q}}(\omega)\big|_{\text{kind}} = \frac{1}{N_k} \sum_{nm\mathbf{k}} \mathcal{G}_{mn\mathbf{k}}^{\lambda\mathbf{Q}}\big|_{\text{kind}} F_{\mathbf{kk-Q}}^{mn\lambda}(\omega), \quad \text{(C1a)}$$

$$F_{\mathbf{kk-Q}}^{mn\lambda}(\omega) = \frac{f_{m\mathbf{k-Q}} - f_{n\mathbf{k}}}{\omega + \epsilon_{m\mathbf{k-Q}} - \epsilon_{n\mathbf{k}} + i0^+}. \quad \text{(C1b)}$$

Now the $\sum_{\mathbf{k}}$ in Eq. (C1a) is represented as a product of sum in the CG and in the FG. The FG can be both a regular or random grid (we used the latter):

$$\Pi_{\lambda\mathbf{Q}}(\omega)\big|_{\text{kind}} = \sum_{\mathbf{K}\in\text{CG}} \sum_{nm} \mathcal{G}_{mn\mathbf{K}}^{\lambda\mathbf{Q}}\big|_{\text{kind}} \frac{1}{N_{\mathbf{K}}N_{\mathbf{K-Q}}}$$
$$\times \sum_{\mathbf{k}\in\text{FG}_{\mathbf{K}}} \sum_{\mathbf{p}\in\text{FG}_{\mathbf{K-Q}}} F_{\mathbf{kp}}^{mn\lambda}(\omega). \quad \text{(C2)}$$

Note here that the FG depends on the CG it was generated from. In particular, N_k is the number of CG points in the Brillouin zone (BZ), while $\sum_{\mathbf{k}\in\text{FG}_{\mathbf{K}}}$ represents a sum over the subset of the FG random k points which are closest to each $\mathbf{K}$ point of the original CG. The number of k points contained in each FG$_{\mathbf{K}}$ subset (which may vary because of randomness and when close to the BZ edge) is $N_{\mathbf{K}}$. For each $\mathbf{K}$ point, the FG subsets around $\mathbf{K}$ and $\mathbf{K} - \mathbf{Q}$ are both needed.

Crucially, both the CG and the FG must undergo convergence tests: a python workflow using the YAMBOPY package was created to automatically generate CG-FG pairs. The numerical evaluation of the delta functions involves the broadening parameter η, which has to be chosen (naturally, as small as possible) according to the densities of the CG and FG grids. In addition, in order to avoid the unnecessary, time- and memory-expensive counting of transitions contributing negligibly, YAMBO automatically selects only transitions satisfying $\varepsilon_{n\mathbf{k}} - \varepsilon_{m\mathbf{k-q}} <= \Omega_{\lambda\mathbf{q}} \pm 3\eta$.

APPENDIX D: CALCULATION FLOW

The *ab initio* phonon linewidth calculation comprises the following six interdependent steps, which are described in
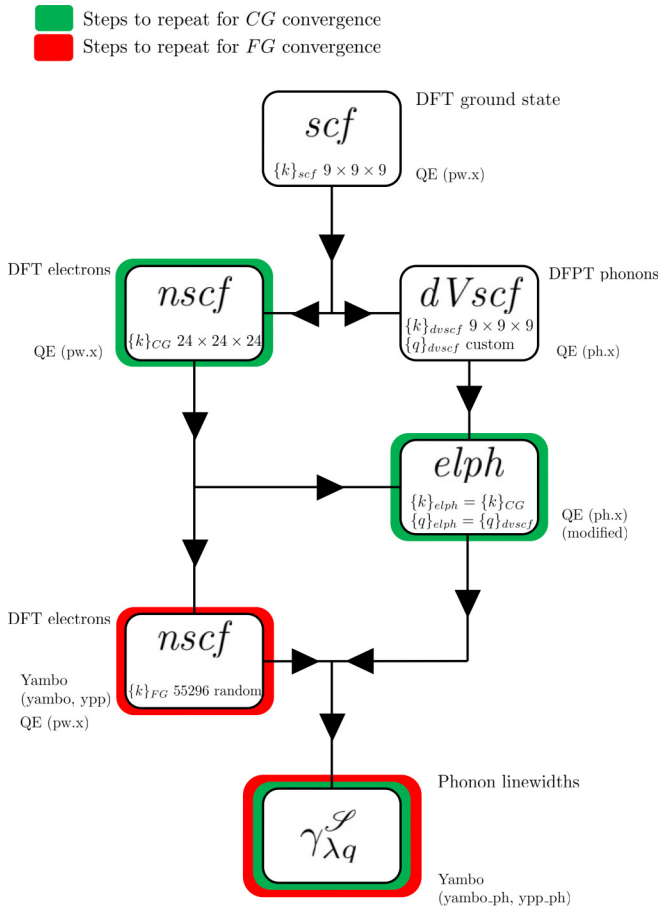
FIG. 10. Linewidth calculation flow discussed in Appendix D. The calculations corresponding to the various steps are shown in boxes. If two boxes are connected by an arrow, it means that the calculation at the ending point depends on the calculation at the starting point. The various calculations may depend on different meshes of reciprocal-space points ({**k**} for electrons, {**q**} for phonons): these meshes are shown in the boxes along with the values used in the case of the MgB$_2$ calculations. On the side of the boxes, additional descriptions of the type of calculations are provided, together with the software package needed (QE or YAMBO) and the specific executables (pw.x, ph.x, yambo, ypp, yambo_ph, ypp_ph) in brackets. The green (red) frame denotes the calculations which depend on the *coarse grid* CG of **K** points (*fine grid* FG of **k** points). See text for more information.

detail in Fig. 10 and are briefly summarized here. In order to give an assessment of the numerical load, the scheme also lists the converged values of the various reciprocal-space grids used to calculate the linewidths in MgB$_2$.

Aside from the **k** and **q** grids an important ingredient of the calculations is the pseudopotential (PP). In this work I tested two kind of PP's: a soft PP and a hard PP. In the soft PP the pseudoboron atom valence comprises the $2p^1$

orbitals, while in the hard case the PP includes also the $2s^2$ levels.

The hard and soft PP's are characterized by two very different wave-function cutoffs: 1200 Ry (hard PP) and 70 Ry (soft PP). A crucial property of the phonon self-energy is that if we look at Eq. (53) we see that, as $C_{\lambda\lambda}^{\text{ref}}$ is a real matrix it follows that it does not contribute to the phonon widths. Consequently, these are more sensible to the details of the calculation, including the kind of PP used.

Indeed, while both PP's yield the same structural and electronic properties, a residual difference remains the case of the phonon widths. In order to estimate this effect let us consider the $\Gamma \rightarrow A$ direction. If we look at the maximum phonon widths along this line we observe that for the E_{2g}^1 state both the screened and overscreened widths change of around 6% when moving from the soft to the hard PP. In the E_{2g}^2 case, instead, the screened case suffers a 25% enhancing, while the overscreened case changes only of the 6%. Finally, while the A_{2u}^{ac} state remains unchanged for both the screened and overscreened widths the screened A_{2u}^{opt} state is quenched when the hard PP is used. The final result is that the message of this work is not at all affected by the use of a soft or hard PP. Still a quantitative evaluation of the phonon widths requires a more careful investigation of the role played by the core levels and the pseudopotential approximation.

Once grids and PP's are selected here it follows the calculation flow:

(i) Self-consistent-field (scf) ground-state calculation using a regular {**k**}$_{\text{scf}}$ grid.

(ii) Derivatives of the scf potential (dVscf) and interatomic force constants calculation using a regular {**k**}$_{\text{dvscf}}$ grid. This fixes the list of phonon momenta **q**, which may be automatically generated (regular grid) or properly chosen.

(iii) Non-self-consistent-field (nscf) calculation. The CG grid used in this calculation defines the **K** points and has to be carefully converged together with the FG grid from step (v) and the broadening parameter η. The grids' convergence can be tested on the phonon linewidth calculations $\gamma_{\lambda\mathbf{q}}$ [step (vi)] looking both at **q** averages along the BZ and at the values at high-symmetry q points. This step also computes the electron energies $\varepsilon_{n\mathbf{K}}$.

(iv) Electron-phonon matrix elements (elph) calculation. In this step, to be run on top of steps (ii) and (iii), the $g_{mn\mathbf{k}}^{\lambda\mathbf{q}}$ are computed.

(v) Second non-self-consistent-field (nscf) calculation. This fixes the FG, which defines the **k** points. Random **k** points are used since they yield faster convergence, and the randomly distributed FG points can be generated with YAMBO. The FG has to be carefully converged together with the CG from step (iii) and the broadening parameter η. It is in this step that the fine-grid electron energies $\varepsilon_{n\mathbf{k}}$ are computed.

(vi) Phonon linewidth calculation. This is the final calculation that yields $\gamma_{\lambda\mathbf{q}}$.

[1] F. Giustino, Rev. Mod. Phys. **89**, 015003 (2017).

[2] R. van Leeuwen, Phys. Rev. B **69**, 115110 (2004).

[3] A. Marini, S. Poncé, and X. Gonze, Phys. Rev. B **91**, 224310 (2015).

[4] S. Poncé, G. Antonius, P. Boulanger, E. Cannuccia, A. Marini, M. Côtè, and X. Gonze, Comput. Mater. Sci. **83**, 341 (2014).

[5] J. Lafuente-Bartolome, C. Lian, W. H. Sio, I. G. Gurtubay, A. Eiguren, and F. Giustino, Phys. Rev. Lett. **129**, 076402 (2022).

[6] H. Fröhlich, Adv. Phys. **3**, 325 (1954).

[7] D. C. Langreth and L. P. Kadanoff, Phys. Rev. **133**, A1070 (1964).

[8] S. Engelsberg and J. R. Schrieffer, Phys. Rev. **131**, 993 (1963).

[9] S. Baroni, P. Giannozzi, and A. Testa, Phys. Rev. Lett. **58**, 1861 (1987).

[10] X. Gonze, Phys. Rev. A **52**, 1086 (1995).

[11] X. Gonze, Phys. Rev. A **52**, 1096 (1995).

[12] S. Baroni, S. de Gironcoli, A. Dal Corso, and P. Giannozzi, Rev. Mod. Phys. **73**, 515 (2001).

[13] M. Calandra, G. Profeta, and F. Mauri, Phys. Rev. B **82**, 165111 (2010).

[14] G. Stefanucci and R. van Leeuwen, *Nonequilibrium Many-Body Theory of Quantum Systems* (Cambridge University Press, Cambridge, 2013).

[15] P. B. Allen, M. L. Cohen, and D. R. Penn, Phys. Rev. B **38**, 2513 (1988).

[16] A. Marini and Y. Pavlyukh, Phys. Rev. B **98**, 075105 (2018).

[17] P. B. Allen, Phys. Rev. B **6**, 2577 (1972).

[18] F. Giustino, J. R. Yates, I. Souza, M. L. Cohen, and S. G. Louie, Phys. Rev. Lett. **98**, 047005 (2007).

[19] I. Errea, M. Calandra, C. J. Pickard, J. Nelson, R. J. Needs, Y. Li, H. Liu, Y. Zhang, Y. Ma, and F. Mauri, Phys. Rev. Lett. **114**, 157004 (2015).

[20] P. B. Allen and B. Mitrović, *Solid State Physics*, Vol. 37 (Academic, New York, 1983), pp. 1–92.

[21] B. Liao, B. Qiu, J. Zhou, S. Huberman, K. Esfarjani, and G. Chen, Phys. Rev. Lett. **114**, 115901 (2015).

[22] Y. Wang, Z. Lu, and X. Ruan, J. Appl. Phys. **119**, 225109 (2016).

[23] Z. Tong, S. Li, X. Ruan, and H. Bao, Phys. Rev. B **100**, 144306 (2019).

[24] A. Gold-Parker, P. M. Gehring, J. M. Skelton, I. C. Smith, D. Parshall, J. M. Frost, H. I. Karunadasa, A. Walsh, and M. F. Toney, Proc. Natl. Acad. Sci. USA **115**, 11905 (2018).

[25] M. Calandra and F. Mauri, Phys. Rev. B **71**, 064501 (2005).

[26] M. d'Astuto, M. Calandra, S. Reich, A. Shukla, M. Lazzeri, F. Mauri, J. Karpinski, N. D. Zhigadlo, A. Bossak, and M. Krisch, Phys. Rev. B **75**, 174508 (2007).

[27] S. Piscanec, M. Lazzeri, F. Mauri, A. C. Ferrari, and J. Robertson, Phys. Rev. Lett. **93**, 185503 (2004).

[28] M. Lazzeri and F. Mauri, Phys. Rev. Lett. **97**, 266407 (2006).

[29] N. Caudal, A. M. Saitta, M. Lazzeri, and F. Mauri, Phys. Rev. B **75**, 115423 (2007).

[30] M. Lazzeri, S. Piscanec, F. Mauri, A. C. Ferrari, and J. Robertson, Phys. Rev. Lett. **95**, 236802 (2005).

[31] M. Calandra, M. Lazzeri, and F. Mauri, Phys. C (Amsterdam) **456**, 38 (2007).

[32] A. M. Saitta, M. Lazzeri, M. Calandra, and F. Mauri, Phys. Rev. Lett. **100**, 226401 (2008).

[33] C. Ferrante, A. Virga, L. Benfatto, M. Martinati, D. De Fazio, U. Sassi, C. Fasolato, A. K. Ott, P. Postorino, D. Yoon, G. Cerullo, F. Mauri, A. C. Ferrari, and T. Scopigno, Nat. Commun. **9**, 308 (2018).

[34] A. Shukla, M. Calandra, M. d'Astuto, M. Lazzeri, F. Mauri, C. Bellin, M. Krisch, J. Karpinski, S. M. Kazakov, J. Jun, D. Daghero, and K. Parlinski, Phys. Rev. Lett. **90**, 095506 (2003).

[35] D. Novko, Phys. Rev. B **98**, 041112 (2018).

[36] Y. Nomura and R. Arita, Phys. Rev. B **92**, 245108 (2015).

[37] X. Tong and M. Bernardi, Phys. Rev. Res. **3**, 023072 (2021).

[38] F. Caruso, J. Phys. Chem. Lett. **12**, 1734 (2021).

[39] H. Tanimura, J. Kanasaki, K. Tanimura, J. Sjakste, N. Vast, M. Calandra, and F. Mauri, Phys. Rev. B **93**, 161203 (2016).

[40] E. Baldini, A. Mann, L. Benfatto, E. Cappelluti, A. Acocella, V. M. Silkin, S. V. Eremeev, A. B. Kuzmenko, S. Borroni, T. Tan, X. X. Xi, F. Zerbetto, R. Merlin, and F. Carbone, Phys. Rev. Lett. **119**, 097002 (2017).

[41] D. Novko, F. Caruso, C. Draxl, and E. Cappelluti, Phys. Rev. Lett. **124**, 077001 (2020).

[42] P. N. Keating, Phys. Rev. **175**, 1171 (1968).

[43] J. Berges, E. G. C. P. van Loon, A. Schobert, M. Rösner, and T. O. Wehling, Phys. Rev. B **101**, 155107 (2020).

[44] D. Novko, Commun. Phys. **3**, 30 (2020).

[45] F. Caruso, M. Hoesch, P. Achatz, J. Serrano, M. Krisch, E. Bustarret, and F. Giustino, Phys. Rev. Lett. **119**, 017001 (2017).

[46] D. Campi, S. Kumari, and N. Marzari, Nano Lett. **21**, 3435 (2021).

[47] G. Strinati, Riv. Nuovo Cimento (1978-1999) **11**, 1 (1988).

[48] G. Onida, L. Reining, and A. Rubio, Rev. Mod. Phys. **74**, 601 (2002).

[49] J. P. Nery, P. B. Allen, G. Antonius, L. Reining, A. Miglio, and X. Gonze, Phys. Rev. B **97**, 115145 (2018).

[50] R. M. Dreizler and E. K. U. Gross, *Density Functional Theory* (Springer, Berlin, 1990).

[51] X. Gonze, P. Boulanger, and M. Côtè, Ann. Phys. **523**, 168 (2011).

[52] J. Nagamatsu, N. Nakagawa, T. Muranaka, Y. Zenitani, and J. Akimitsu, Nature (London) **410**, 63 (2001).

[53] H. J. Choi, D. Roundy, H. Sun, M. L. Cohen, and S. G. Louie, Nature (London) **418**, 758 (2002).

[54] E. R. Margine and F. Giustino, Phys. Rev. B **87**, 024505 (2013).

[55] A. Floris, G. Profeta, N. N. Lathiotakis, M. Lüders, M. A. L. Marques, C. Franchini, E. K. U. Gross, A. Continenza, and S. Massidda, Phys. Rev. Lett. **94**, 037004 (2005).

[56] A. Q. R. Baron, H. Uchiyama, Y. Tanaka, S. Tsutsui, D. Ishikawa, S. Lee, R. Heid, K.-P. Bohnen, S. Tajima, and T. Ishikawa, Phys. Rev. Lett. **92**, 197004 (2004).

[57] D. Karlsson, R. van Leeuwen, Y. Pavlyukh, E. Perfetto, and G. Stefanucci, Phys. Rev. Lett. **127**, 036402 (2021).

[58] P. Giannozzi, O. Andreussi, T. Brumme, O. Bunau, M. B. Nardelli, M. Calandra, R. Car, C. Cavazzoni, D. Ceresoli, M. Cococcioni, N. Colonna, I. Carnimeo, A. D. Corso, S. de Gironcoli, P. Delugas, R. A. D. Jr, A. Ferretti, A. Floris, G. Fratesi, G. Fugallo *et al.*, J. Phys.: Condens. Matter **29**, 465901 (2017).

[59] D. Sangalli, A. Ferretti, H. Miranda, C. Attaccalite, I. Marri, E. Cannuccia, P. Melo, M. Marsili, F. Paleari, A. Marrazzo, G. Prandini, P. Bonfà, M. O. Atambo, F. Affinito, M. Palummo, A. Molina-Sánchez, C. Hogan, M. Grüning, D. Varsano, and A. Marini, J. Phys.: Condens. Matter **31**, 325902 (2019).

[60] The distribution I used is available at this address: https://github.com/QEF/q-e/releases/tag/qe-6.6.

[61] The YAMBO distribution is available here, https://github.com/yambo-code/yambo/releases/tag/5.0.2, while the experimental *yambopy* package is here, https://github.com/yambo-code/yambopy.